A Proposal for a Long Baseline Oscillation Experiment Using A High Intensity Neutrino Beam from the Fermilab Main Injector to the IMB Water Ĉerenkov Detector. FNAL P805

W. Gajewski, P.G. Halverson, W.R. Kropp,
S. Matsuno, C. McGrew, L.R. Price, F. Reines,
J. Schultz, H.W. Sobel
University of California, Irvine

D. Casper, S.T. Dye, L.R. Sulak, F. Witt
Boston University

M. Goldhaber
Brookhaven National Laboratory

C.B. Bratton
Cleveland State University

R. Becker-Szendy, J.G. Learned
The University of Hawaii, Manoa

T.W. Jones
University College, London

R. Miller, R. Svoboda
Louisiana State University

T.J. Haines
The University of Maryland

R. Cady, J.M. LoSecco
The University of Notre Dame

D. Kielczewska
Warsaw University, Warsaw

October 1990

Abstract

We propose to study muon neutrino oscillations by detecting in the IMB detector neutrinos produced by a proton beam from the Main Injector at Fermilab. The distance between the beam source and the detector is 570 km. The interactions span the energy range up to about 60 GeV with a mean of about 13 GeV.

We are able to detect the muon neutrino disappearance of more than 2%, which together with the L/E ratio of 43.8km/GeV makes the experiment sensitive to the range of mass squared difference $\delta m^2 \approx \text{few} \times 10^{-3}(\text{eV})^2$. This range is a two order of magnitude improvement over the existing limits from the CHARM experiment.

The experiment will probe a region which has been well motivated by both experimental hints from the observation of atmospheric neutrinos ("Kamioka effect") and theory (flipped SU(5)).

By taking advantage of the well studied characteristics of the IMB detector for searching for nucleon decay and atmospheric neutrino interactions, we have the ability to unambiguously discriminate between oscillation to electron or tau neutrinos. We can positively identify charged current electron neutrino interactions above the lepton energy of 10 GeV.

If muon neutrino disappearance were observed, this would allow identification of the flavour to which muon neutrinos have oscillated.

Contents

List of Figures

List of Tables

1 Physics Motivation of the Experiment

The high intensity neutrino beam from the Main Injector at FNAL presents an opportunity to conduct a long baseline ν_μ oscillation experiment. Some indications of such oscillation have been reported by the underground proton decay detectors [1][2][3][4]. An apparent depletion of low energy muon neutrinos in the atmospheric neutrino beam, of the order of 40%, has been reported by the Kamiokande group. Analyses of this result, in conjunction with other limits on neutrino oscillation and with the solar neutrino problem, were conducted by several authors [5][6]. These analyses lead to the conclusion, that while the electron neutrino, of a very small mass ($m_{\nu_e} \sim (10^{-9} - 10^{-6})$eV), is very weakly mixed with the other neutrinos, the tau neutrino can acquire a substantial mass ($0.17eV < m_{\nu_\tau} < 0.63$eV) and be strongly mixed with the muon neutrino of intermediate mass ($m_{\nu_\mu} \sim (0.3-2)\times 10^{-3}$eV). The elements of the neutrino mixing matrix have been deduced by Learned et al. as follows:

$$\begin{pmatrix} \nu_e \\ \nu_\mu \\ \nu_\tau \end{pmatrix} = \begin{pmatrix} 1. & 0.087 & \epsilon \\ -0.066 & 0.755 & 0.656 \\ -\epsilon' & -0.656 & 0.755 \end{pmatrix} \begin{pmatrix} \nu_1 \\ \nu_2 \\ \nu_3 \end{pmatrix}$$

with ϵ, $\epsilon' \ll 1$. Here ν_e, ν_μ, ν_τ are the gauge eigenstates, and ν_1, ν_2, ν_3 - the mass eigenstates. A reasonable see-saw mechanism for the mass hierarchy of lepton families has been assumed in this analysis. The authors point out that with such a mixing matrix, one should observe a dramatic effect of muon neutrino depletion in a detector at a distance of $L/1\text{km} > 25 \times E/1\text{GeV}$!

However, the observation of such strong depletion of low energy muon neutrinos, as reported by the Kamiokande group, has not been confirmed by the other underground detectors (IMB and Frejus). Nonetheless, both these groups do observe some, of the order of 10-20%, deficit of muon signal with a statistical error of the size of the deficit. Such a result, according to a Barger and Whisnant calculation, substantially widens the allowed region of neutrino mass-square differences and mixing with respect to that derived from the Kamiokande result. This region however is still testable by experiments fulfilling the condition $L > 25 \times E(\text{km/GeV})$.

It is interesting to point out that the new GUT, "flipped" $SU(5)\times U(1)$

[7], derived from string theory, with reasonable parameterization, leads to similar conclusions. From the superpotential, invariant under the symmetry of this model, one can extract mass matrices of the fermion families. They acquire, in a natural way, a see-saw mechanism. For neutrinos, the model predicts the masses $m_{\nu_e} \sim 10^{-7}$eV and m_{ν_μ}, $m_{\nu_\tau} < 1$eV, and no mixing of electron neutrinos with the other neutrino species. Reasonable assumptions for the GUT scale and Yukawa couplings provide a final neutrino mixing matrix surprisingly close to the one derived by Learned et al.:

$$\begin{pmatrix} \nu_e \\ \nu_\mu \\ \nu_\tau \end{pmatrix} = \begin{pmatrix} 1. & \sim 0. & \sim 0. \\ \sim 0. & 0.78 & 0.62 \\ \sim 0. & -0.62 & 0.78 \end{pmatrix} \begin{pmatrix} \nu_1 \\ \nu_2 \\ \nu_3 \end{pmatrix}.$$

The results of the "flipped" GUT indicate that the measurement of the neutrino oscillation parameters provide a direct test of the Grand Unification Theories. It might turn out that the fermion mass structure and their mixing would be the only window available to the grand unification energy scale.

1.1 Goals of the Experiment

If the analysis of the existing oscillation data and the predictions of the theory are correct, there is an opportunity to observe ν_μ disappearance and ν_τ appearance at the optimal distances $L > 25 \times E$km/GeV. This condition, by fortuitous accident, is realized by the neutrino beam produced at Fermilab by the Main Injector passing to the IMB detector.

A major goal of the experiment described in this proposal is to resolve the ambiguities implied by the deficit of muon neutrinos coming from the atmosphere. It can provide either a proof of the neutrino oscillation or new limits on the neutrino mass-square difference two orders of magnitude below the limits currently explored, and the mixing ($\sin^2(2\theta)$) above a few $\times 10^{-2}$. If the oscillation were observed, it could also indicate which neutrino species were involved in such an oscillation. These goals can be achieved by replacing the atmospheric neutrino beam with a well understood and controlled accelerator beam, traversing a well known path between the accelerator and the detector.

1.2 Comparison of the Proposed Experiment with the Studies of Atmospheric Neutrinos

The IMB detector has been extensively used to study neutrino oscillations using the flux of neutrinos produced by cosmic rays in the atmosphere [4].

There are several disadvantages to such studies. The atmospheric neutrino flux in the lower energy part of its spectrum is calculated with systematic uncertainties of the order of 20-30%. The calculations are based on poorly known fluxes, spectra and composition of the primary cosmic ray beam striking the atmosphere. Further, they involve models for production of secondaries in interactions of cosmic rays with nuclei of the atmosphere. The emerging muons have enough range to decay in flight. As a result of all these processes, the neutrino spectrum falls as E^{-3} and consists of a comparable number of electron and muon neutrinos. Since the neutrino energies are mainly below 1 GeV, calculation of their interactions in the detector involve not very well understood nuclear cross sections. The composition of the neutrino flux creates a very high background for studies of oscillations $\nu_\mu \leftrightarrow \nu_e$. All these conditions preclude an experiment with a systematic precision better than 10-20%.

Furthermore, the event rate for atmospheric neutrino interactions, even in a detector the size of IMB, is very low. It would take more than 10 years of livetime with the natural atmospheric source to achieve the contained event statistics of a few thousand events. It would take 30 years of live time to get a comparable sample of neutrino induced entering muons.

Instead, in the proposed experiment, the cosmic ray flux is replaced by a single proton beam, of well defined energy, interacting in a well understood target. Neutrinos emerge mainly from decays of pions and kaons produced in the target in a well defined space. Their intensity and spectrum can be calculated with higher precision, their direction, and the distance they travel to the detector are well defined. All these factors create conditions for an experiment with a systematic precision improved by a factor of 10.

2 Layout of the Experiment

To perform the experiment we employ the muon neutrino beam produced by 120 GeV protons from the main injector at FNAL, and as a target the existing and well understood IMB water Čerenkov detector. The path of the beam is shown in fig. 1. The FNAL accelerator has a geographical latitude of 41.5° N and a longitude of 88.15° W. The IMB detector is situated in a salt mine, 600 m underground, at Grand River, Ohio, at latitude 41.756° N and longitude 81.286° W. The great circle angle between the beam source and the detector is 5.13° (89.6 mrad), and the linear distance is 570 km. The beam at FNAL has to point almost east and underground with an angle of 44.8 mrad with respect to the horizon. As will be shown later, the beam has to be aimed at the detector with an accuracy of about 0.2 mrad. Such accuracies are easily achievable by means of the military GPS system, which allows measurement of geographical coordinates with a precision of 1 cm. One of the institutions involved in our experiment, Louisiana State University, has acquired the equipment necessary to apply this system.

2.1 Beam Design

We have developed a design of the neutrino beam line which can withstand the full capacity of the proton beam produced by the Main Injector and maximize the neutrino output per incident proton using the fixed, short length (300m) of decay pipe. This beam fulfills the requirements of both short baseline (P803) and long baseline (IMB-P805) oscillation experiments. The layout of the beam, from the physics perspective, is described in detail in Appendix A of this proposal and, from the engineering point of view in the Conceptual Design Report of the FNAL Research Division. The neutrino output of this beam line has been calculated using the program described in Appendices B and C. The most important characteristics of this beam for the proposed experiment are:

1. neutrino flux at the distance of IMB, $10^4\nu/m^2/10^{13}$ ppp.
2. mean neutrino energy along the beam axis, 13.2 GeV.
3. the beam spectrum (see fig.2).

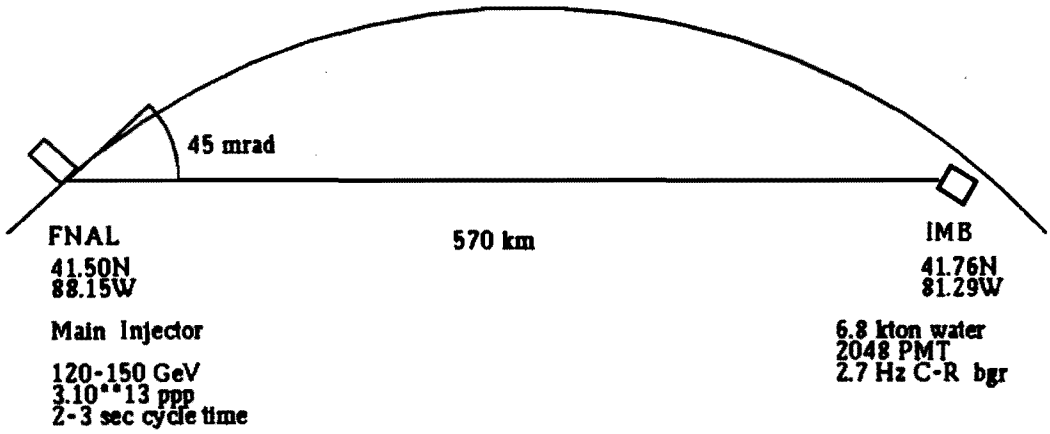

Figure 1: Schematic of neutrino beam traveling from FNAL to the IMB detector.

4. variation of the mean energy with angle (see fig. 3).

5. variation of the beam flux with angle (see fig. 4).

6. beam contamination by other neutrinos:

   - muon antineutrinos $\approx 1.5\%$
   - electron neutrinos and antineutrinos $\approx 0.5\%$

This design, by no means final, still has some room for further improvements. Nevertheless, the neutrino beam produced by this line has been used for the analysis of different systematic uncertainties involved in the proposed experiment. When the final design is implemented, the results of this analysis should change by no more than 10-20%.

2.2 The role of the Close Detector (P803)

As shown in Appendix C, the calculation of the beam's neutrino output is based on a very crude assumption about the $p + C$ interactions. Nuclear inclusive cross sections for the channels of major interest, i.e. for π^+ and K^+ production, have not been measured for a sufficiently large range of Feynman x, especially for $x < 0.3$. The measurements of the p_t dependence of these cross sections are more sparse. This situation is directly reflected in the accuracy of the results of the beam calculation. While the region of the neutrino spectrum populated by higher energy pions and kaons is reliable on the level of accuracy of the cross section measurements ($\approx 10\%$), the region due to low energy pions and kaons is only good to the accuracy of the assumed extrapolation of the measured cross sections. To get more reliable predictions, one would have to conduct extensive measurements of the required missing data.

Another solution, more precise, is to situate a detector of high spatial and energy resolution on the same beam line, close to the end of the decay pipe. Such a detector can, with sufficient accuracy and high efficiency, provide the necessary data on the neutrino interactions. These data can then be used to tune the beam Monte Carlo, so it can give the beam characteristics extrapolated to the beam axis with the required precision.

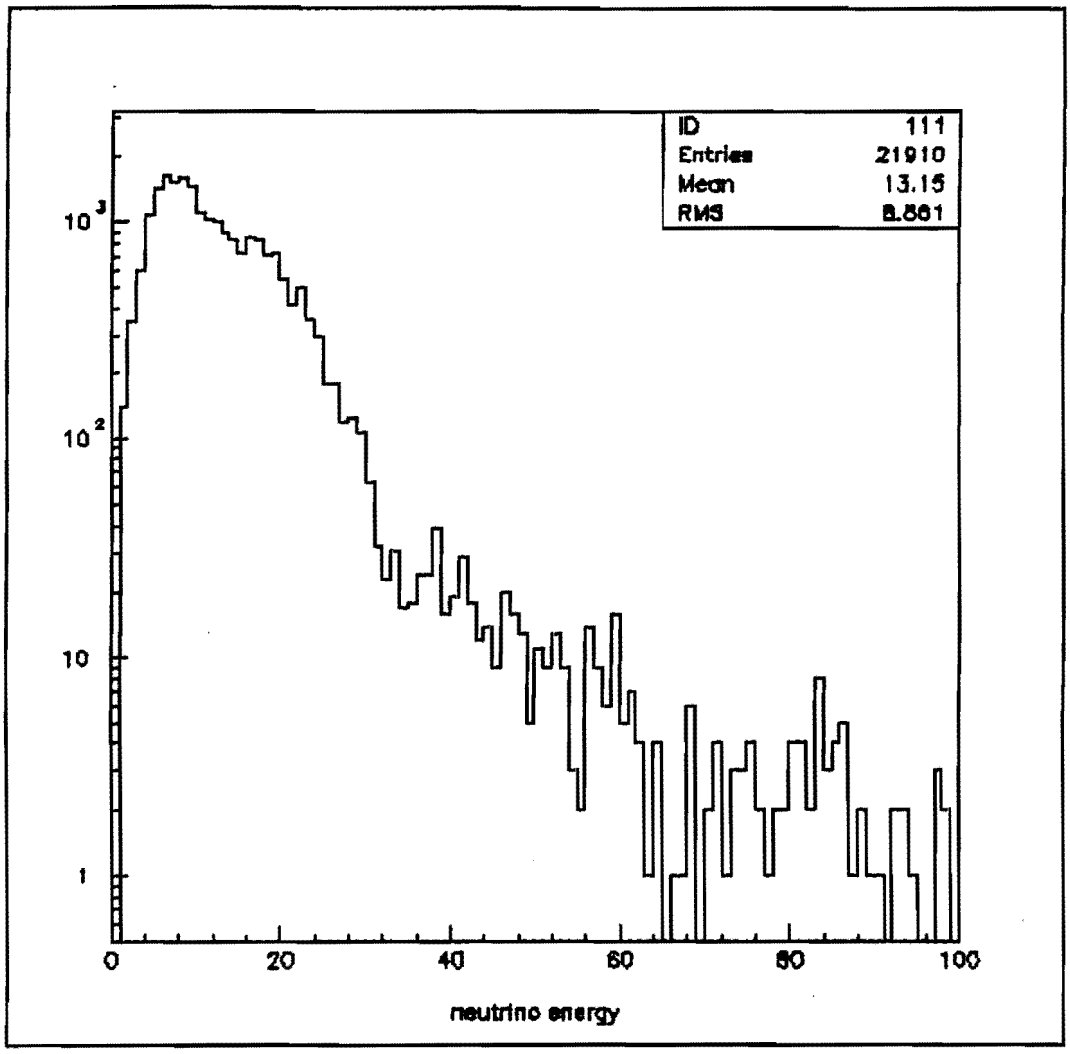

Figure 2: Energy spectrum of the neutrino beam.

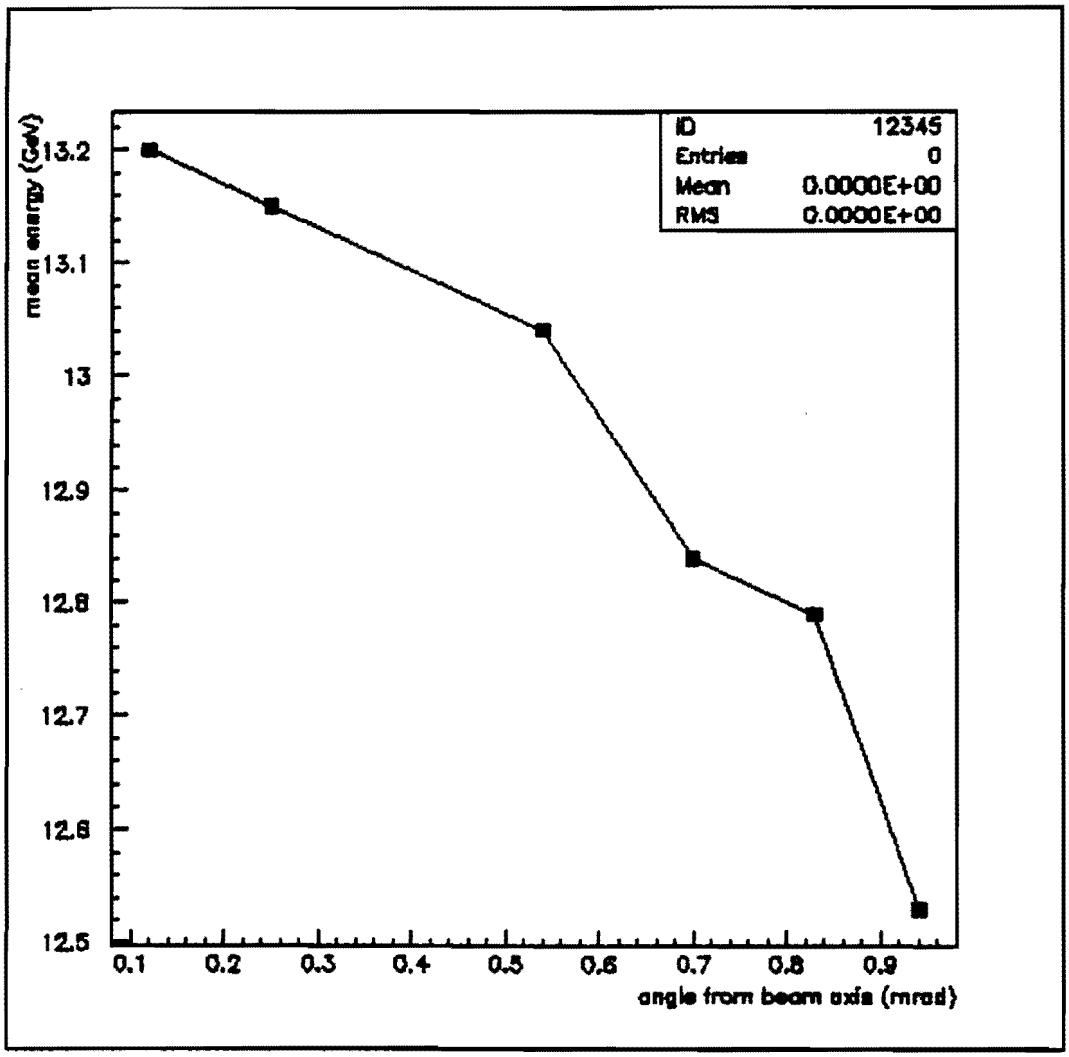

Figure 3: Variation of the mean neutrino energy as a function of angle from the beam axis.

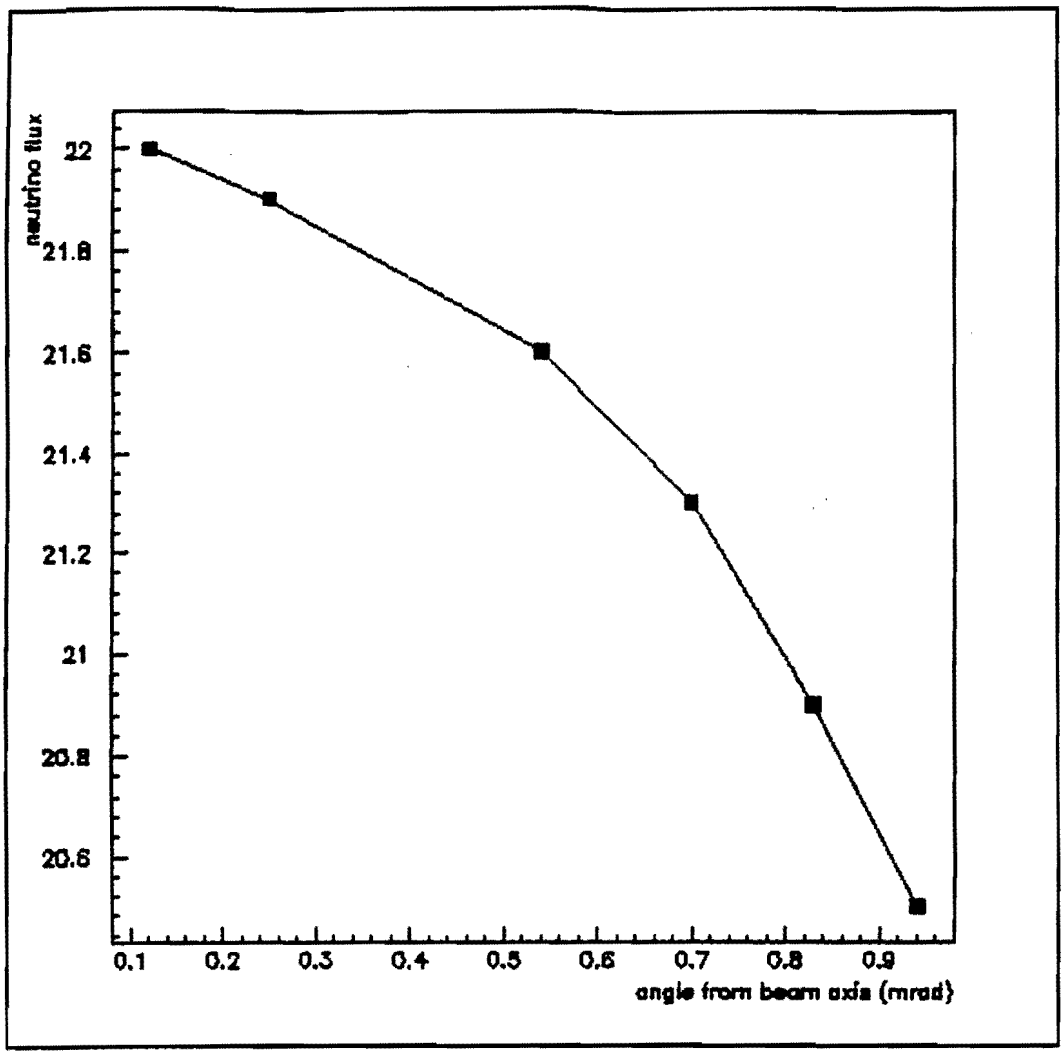

Figure 4: Variation of the beam flux as a function of angle from the beam axis.

We propose that the role of this close detector be carried out by the short baseline oscillation experiment P803. We believe that without such a close neutrino detector the predictive power of the beam Monte Carlo is not sufficient to assure the systematic precision of the experiment for which we are aiming. We consider duplication of almost the entire P803 detector uneconomical. The validity of our proposal rests on the use of the P803 detector, on the same beam line.

2.3 Features of the IMB detector

The detector consists of a rectangular volume of size 17m × 17.5m × 23m filled with highly purified water (see fig 5). That volume is viewed from its surface by 2048 8" Hamamatsu photomultiplier tubes (PMT), each of which is instrumented with a 2'x2' waveshifter plate. Such an arrangement provides a sensitivity of 1.2 photoelectrons collected per 1 MeV energy deposited by charged particles in the detector volume. The trigger threshold of 10 MeV is far below the requirements of the discussed experiment.

The 2.7 Hz background rate of cosmic ray muons passing through the detector with a dead time of 3.5 ms per trigger provides a comfortable live time of 99%.

The absolute time of every trigger is measured by a GEOS clock with an accuracy of 0.5 ms. A local crystal provides a relative timing with the accuracy of 3 μs. These clocks provide sufficient precision to make gating of the accelerator spill unnecessary. However, we shall need an additional set of similar clocks and a tape station for recording times of accelerator spills at Fermilab for the off-line analysis of the data. With such an arrangement, we shall be able to perform the oscillation experiment with no interference with the other goals of our physics program.

The detector is triggered by interactions taking place in its volume and by entering tracks. The position of a light–producing track can be reconstructed from the measured times when phototubes sense the light and from the pattern of the illuminated tubes. Reconstruction of events with a spherical light output is accurate to within 0.5 m, and the beginning of a single track is accurate to within 1.5 m. Tracks entering the detector produce a pattern of early tubes with large pulse height (the so called "entry spot") which makes them easily distinguishable from contained interactions.

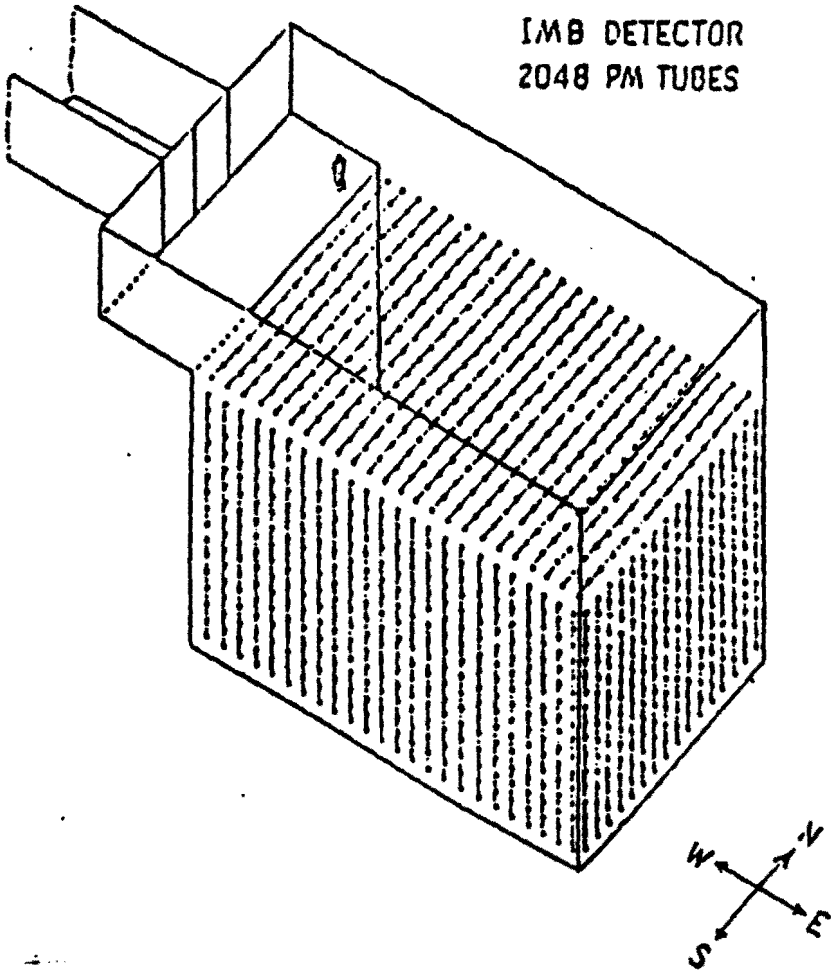

Figure 5: Schematic of the IMB detector.

The detector provides some identification of leptons produced in neutrino interactions. Sixty percent of the negative muons stopping in the detector produce a decay electron signal. Muons with energy above about 4 GeV produce patterns of lit tubes visually distinguishable from the patterns produced by electrons. Muons of such an energy traverse the whole detector, giving the pattern of an exiting track, while the electron shower deposits its whole energy in the detector, illuminating many tubes, but leaving a ring of tubes with a very high pulse height of the size of a few radiation lengths in water. To illustrate this, fig. 6 shows patterns of lit tubes produced by a muon track and an electron track, both of energy 10 GeV.

Below such energies, more elaborate methods of pattern analysis provide distinction between showering tracks (like electrons or π^0s) and nonshowering tracks (like muons or charged pions) with a reliability of about 90%. These techniques have been developed over several years for use in proton decay and atmospheric neutrino studies.

Neutral pion tracks are clearly resolved from electron tracks up to energies of 500 MeV, because the showers of the individual gammas are then separated by more than 30°. Above this energy, some identification is possible, with the confidence diminishing with increased energy.

The layout of the detector and of the adjacent laboratory are shown in figures 7 and 8. The neutrino beam will strike the detector from the West, almost perpendicularly to one of the walls (the West wall). It will also come from below, with an incident angle of 2.6° below the horizon. For the purpose of the proposed experiment, as discussed later, it is important to know the structure of the rock surrounding the detector, about 200 m to the west, 25 m below and above. This structure is known from the geological profile in the vicinity of our detector, provided to us by the Morton-Thiokol Co.

2.4 Event Rate at the IMB detector

If we assume that the Main Injector is able to provide 3×10^{13} ppp with a repetition time of 2 sec and that our beam simulation predicts correctly the neutrino flux at the distance of the IMB detector, we can expect the

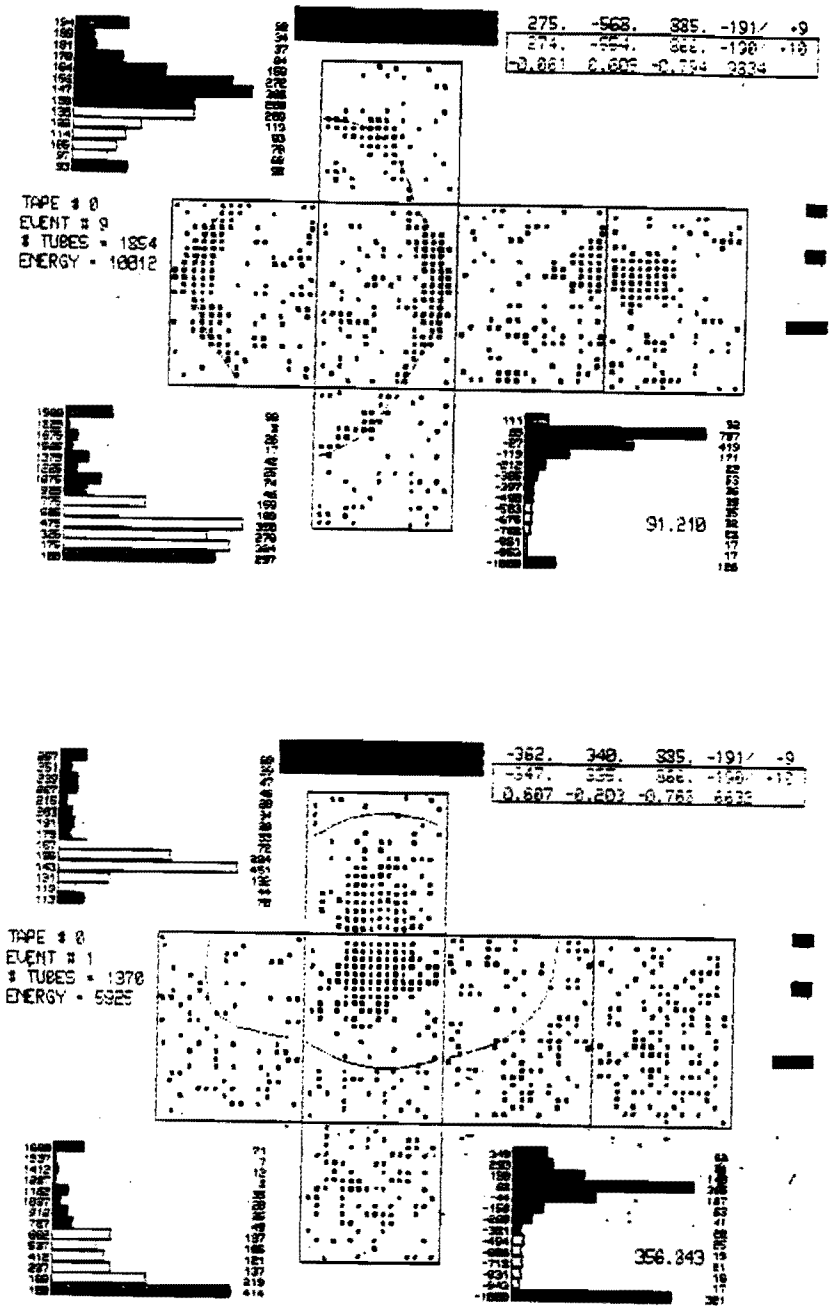

Figure 6: Hit pattern for an elctron (upper portion of figure) and for an muon. Both particles have 10 GeV of energy and enter the detector from the top.

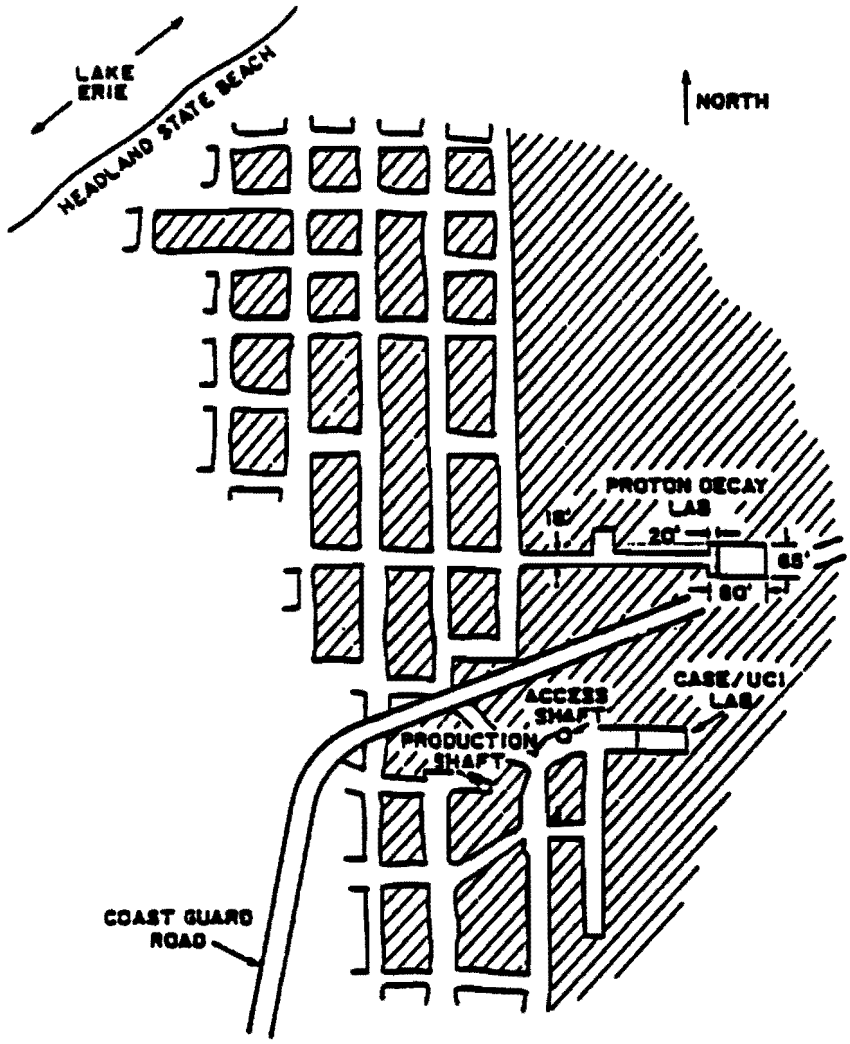

Figure 7: Plan of the Morton-Thiokol salt mine in the vicinity of the IMB laboratory. Note that the chamber marked as "CASE/UCI Lab" can accommodate another large neutrino detector.

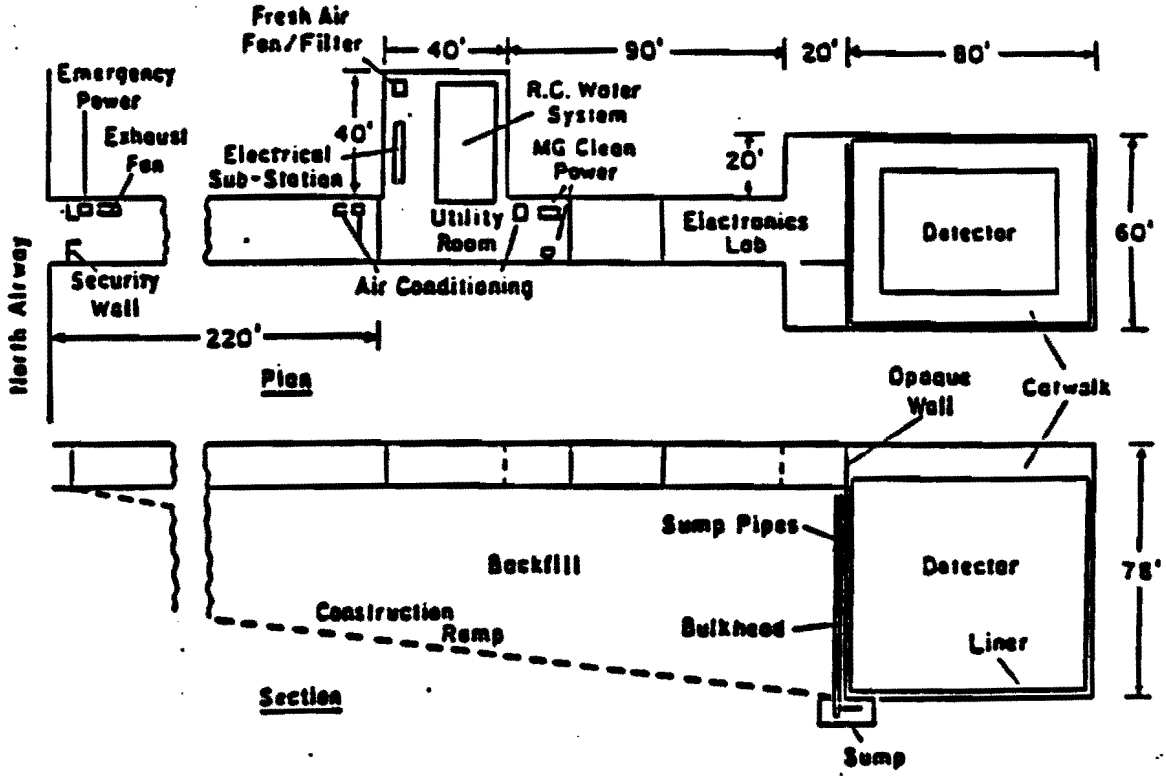

Figure 8: Layout of the IMB detector and the adjacent laboratory

following rate of neutrino interactions in the detector:

$$\left(\begin{array}{c}\text{Avogadro's}\\ \text{Number}\end{array}\right)\left(\begin{array}{c}\text{Target}\\ \text{Mass}\end{array}\right)\left(\frac{\sigma^{cc}_{Tot}}{E_\nu}\right)\langle E_\nu\rangle\left(\frac{cc+nc}{cc}\right)$$
$$\times\left(\frac{\nu\ \text{flux}}{10^{13}\text{ppp}}\right)\left(\frac{\text{ppp}}{10^{13}}\right)\left(\frac{\text{pulse}}{\text{hour}}\right)$$
$$= \left(\frac{6\times10^{23}}{\text{g}}\right)(6.8\times10^{9}\text{g})\left(\frac{0.67\times10^{-38}\text{cm}^2}{\text{GeV}}\right)(13\text{GeV})(1.3)(1/\text{cm}^2)(3)\left(\frac{1800}{\text{hour}}\right)$$
$$= \text{2.6 events per hour.}$$

Thus, in a half year (25 weeks, 100 hours per week) we can collect a sample of 6500 events. A sample of this size assures 1.3% statistical accuracy, better than the expected systematic uncertainties of the experiment.

In addition to the contained events, the detector collects muons produced by charged current neutrino interactions in the surrounding salt. The effective target mass for interactions producing muons, which would enter the detector through the West wall can be roughly estimated from the formula:

$$M_{\text{effective}} = \text{vol}\times\rho = S\langle E_\nu\rangle\langle y\rangle\frac{\rho}{\frac{dE}{dx}\rho}$$

where ρ is the density of the rock, $S = 300\text{m}^2$ is the surface area of the West wall, $< E_\nu >= 19.7\text{GeV}$ is the mean energy weighted by the interaction cross section, $< y >= 0.5$ is the fractional average energy transfer to the muon, and $dE/dx = 2\text{MeV/g/cm}^2$ is the energy loss by a muon in rock.

It is important to notice that this mass depends on the type of matter only through the energy loss dE/dx which does not vary much from one type of rock to another.

Substituting the above values one gets the target mass of 14.8 kton. This target mass provides 4.4 muon tracks per hour recorded in the detector.

A more realistic Monte Carlo, described in some detail in Appendix D, indicates that for muons entering the detector through all walls, the effective target mass is 17.8 kton which corresponds to a rate of 5.2 muon tracks entering the detector per hour. In half a year we could collect a sample of 14000 such events.

2.5 Background to the Accelerator Induced Signal

The only background to the contained event signal from the accelerator neutrinos is due to atmospheric neutrinos. This background is negligible for a number of reasons. The ambient rate of contained events at IMB is about 1.3 per day. In addition, the accelerator neutrinos will have a duty factor of 10^{-3} compared to 1 for the ambient rate. The accelerator events come from a specific direction whereas the ambient rate is almost isotropic. These factors imply an ambient background of about 10^{-6} per event. Atmospheric events are also usually of lower energy than the ones induced by the accelerator neutrinos.

The sample of entering muons will also have a much higher rate than that from the external ambient neutrino interactions of 0.5 events per day. However, because the accelerator beam is near the horizon, some muons coming from the surface may be mistaken for the accelerator induced neutrino interactions. Nevertheless, a rough estimate, using the duty factor of 10^{-3} indicates a background from this source to be about 10^{-6} per entering track.

3 Search for Neutrino Oscillation

3.1 Muon Neutrino Disappearance

The first indication of muon neutrino oscillation would be their disappearance from the beam. We propose to look for such a disappearance in three different ways, each being subject to different systematic limitations:

1. We can compare the rate of contained events and the rate of entering muons with those predicted from the beam characteristics.
2. We can measure the ratio of the number of muons entering the detector to the number of contained events. This ratio does not depend on the flux of the neutrino beam.
3. We can measure the fraction of contained events classified as having a muon track. This method, applied by us to study interactions of atmospheric neutrinos, seems to be well suited for events produced by neutrinos from the lowest part of the energy spectrum. Such interactions can be totally contained in the detector, providing measurements of the total energy and identification of the individual tracks.

3.1.1 The rate of contained events

The number of neutrino interactions taking place in the volume of the detector depends on the following factors:

1. The flux of each kind of neutrino.
2. The cross section for both charged and neutral current interactions of each neutrino species in water.
3. The fiducial volume of the detector.

It is necessary to stress here a significant difference between the expected number of contained events for various oscillation scenarios. When muon neutrinos change to some noninteracting neutrinos like right–handed neutrinos ν_R, they produce neither charged nor neutral current events. The

signal of the contained events vanishes in proportion to the oscillation probability. On the other hand, when muon neutrinos oscillate to electron neutrinos, the number of the contained events does not change because the cross sections for charged and neutral current interactions for both these neutrinos is the same. The intermediate situation is for the oscillation to tau neutrino: the neutral current cross section for muon and tau neutrinos is the same, but the charged current cross sections are different. Due to the τ lepton mass, the charged current cross section for tau neutrino has a higher threshold and rises more slowly than for muon neutrino. The ratio of ν_τ(cc) and ν_μ(cc) cross sections is shown in fig. 9.

The primary limitation in predicting the number of contained events is due to the uncertain knowledge of the beam characteristics. As has been mentioned, due to the lack of experimental data for secondary production in the target, the predictive power of the beam Monte Carlo in terms of the absolute flux is not better than 10%. Using the data from the close detector we hope to improve this precision by at least a factor of 2-3.

The second limitation is due to the accuracy of aiming the beam toward the detector. We discuss this problem later, however its contribution in absolute terms seems to be smaller.

To summarize, we believe that we can detect the eventual total disappearance of neutrino interactions at a level of 5% or better.

3.1.2 The rate of muons entering the detector

The number of muons entering the detector from neutrino charged current interactions in the surrounding rock can be calculated following the scheme described in Appendix D. That number depends mainly on the following factors:

1. The flux of muon neutrinos and anti-neutrinos in the beam.
2. Their charged current cross section in the material surrounding the detector.
3. The energy spectrum of the secondaries produced in such interactions, especially of the muons, which is directly related to the energy spectrum of neutrinos in the beam.

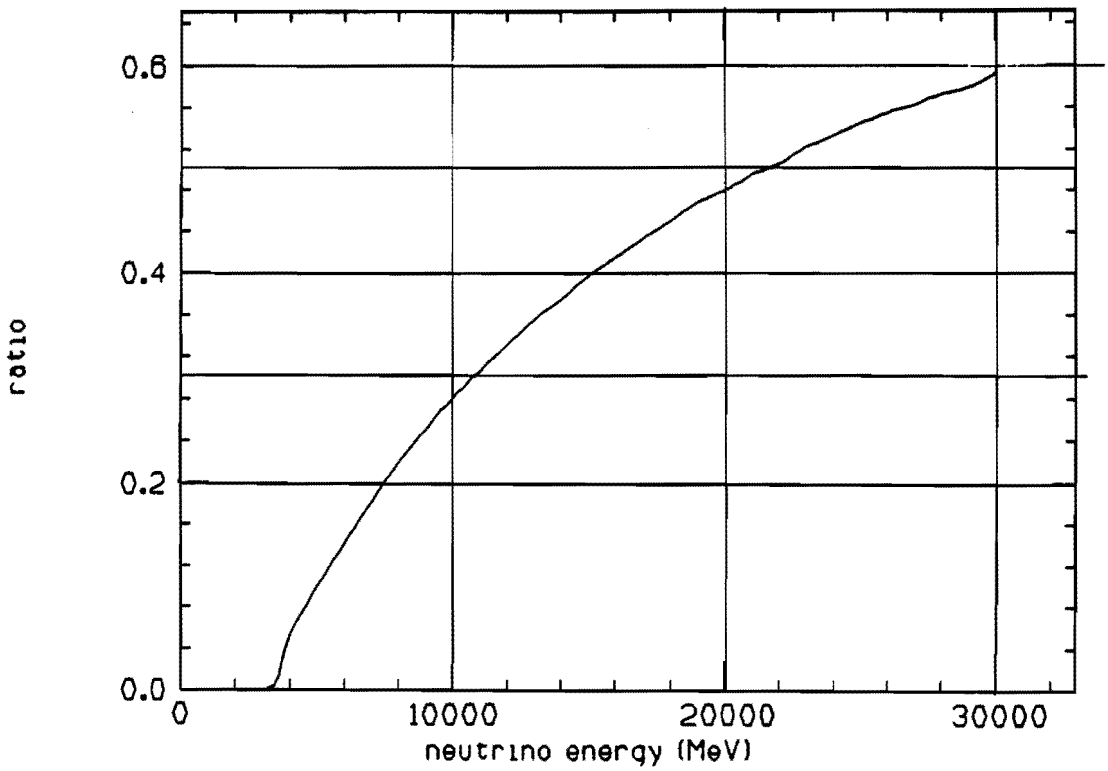

Figure 9: The ratio of ν_τ(cc) and ν_μ(cc) cross sections.

4. The geometry of the detector and its surrounding, and properties of the surrounding matter.

The first factor of this list cancels the similar one which determines the number of contained events in the detector.

Fig. 10 shows the distribution of muon ranges in the salt before they enter the IMB detector. As one can see from the figure, it is necessary to know precisely the geometry of the target within about 120m to the West of the detector and about 10m above and below. All this information is available from the records of the wall structure taken when the detector was built, and from the geological profile provided to us by the Morton-Thiokol Co, taken in the vicinity of our detector.

All man-made voids, like labs and utilities which happen to be built on the west side of the detector, are well documented and easy to implement in the GEANT program. Most of them are on a level above the top of the detector. This region does not produce a significant signal from the neutrino beam arriving at the detector from below the horizon.

The oscillations of muon neutrinos to any other kind of neutrino species always decreases the number of observed entering muon tracks with respect to the predicted number, independent of the different oscillation scenarios.

3.1.3 Systematic effects involved in measurement of the number of entering muons

The main source of systematic uncertainty in the measurement of the number of entering muons is misidentification of contained and entering tracks. To deal with this uncertainty we plan to use a signature of the "entry spot" together with an active veto. This active veto will be developed and tested in the coming years.

Another source of systematic uncertainty is the hadronic component of the neutrino interactions. Most of the pions are absorbed in the rock and do not enter the detector; however, some are not absorbed and simulate a muon track. The admixture of this kind of hadronic track has been calculated following the method described in Appendix D.

We have found that only about 4% of tracks entering the detector are due to hadron tracks from charged and neutral current interactions which

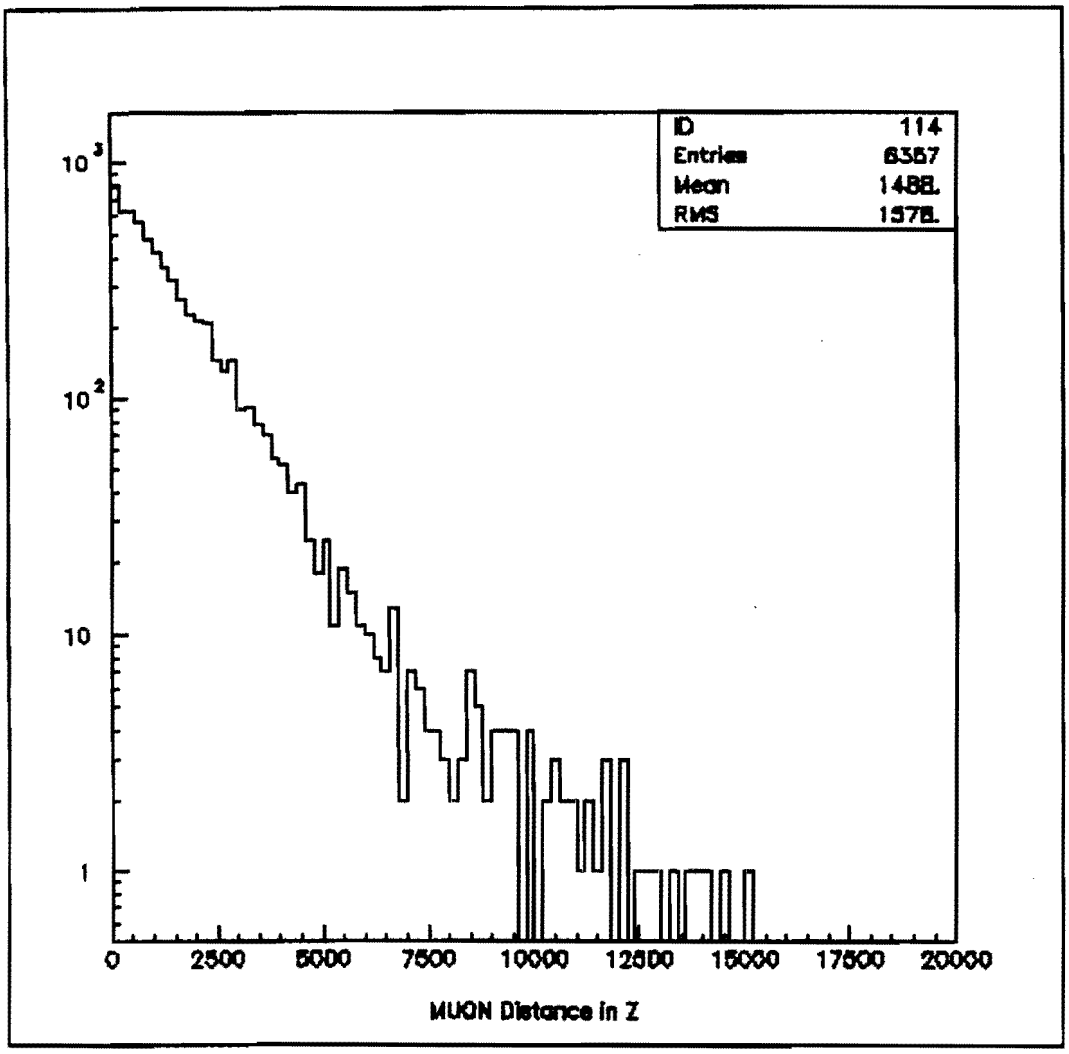

Figure 10: The distribution of muon range in the salt before the muons enter the detector

are not accompanied by a muon track. Even if this estimate of entering pion tracks is incorrect by several percent, it does not introduce an error in the measurement of the number of entering muon tracks of more than 1%. The energy distribution of the entering tracks is shown in fig. 11. As one can see, the hadronic contamination of the muon tracks is at lower energy, so most of these tracks stop in the detector. Our capability of recording the muon decay electron should be helpful in substantially diminishing the contamination from negative pions.

The most serious uncertainty in the measurement of the number of entering muons is due to the uncertainty in the aiming of the neutrino beam toward the detector. As has been previously shown, the characteristics of the beam change with the angle between the beam axis and the direction to the detector: both the flux and the mean energy of the neutrinos decrease with increasing angle. While the influence of changes in the flux cancel in the ratio with the rate of contained events, the changes of the spectrum cause sizable changes in the effective target mass for entering muons.

Folding in the expected neutrino spectra obtained with the program described in Appendix B, with the chain of programs from Appendix D one obtains the variations of the effective target mass shown in fig. 12. This figure, together with fig. 3, shows that the designed beam has a "flat top", with small variations of the beam characteristics up to about 0.5 mrad. Within this region the "effective target mass" changes by less than 1%. Missing the detector by 1 mrad produces an effect on the order of 6%. These considerations prove that an aiming accuracy for the beam of 0.2 mrad is sufficient to control the error introduced by variations in the beam characteristics. As we mentioned before, such accuracy should be easily attainable with current surveying methods.

In summary, we have not identified any effect which would introduce systematic uncertainties larger than 1% into the measurement of the ratio of entering muons to the number of contained events. We believe that we can achieve an overall accuracy of this parameter of the order of 2%.

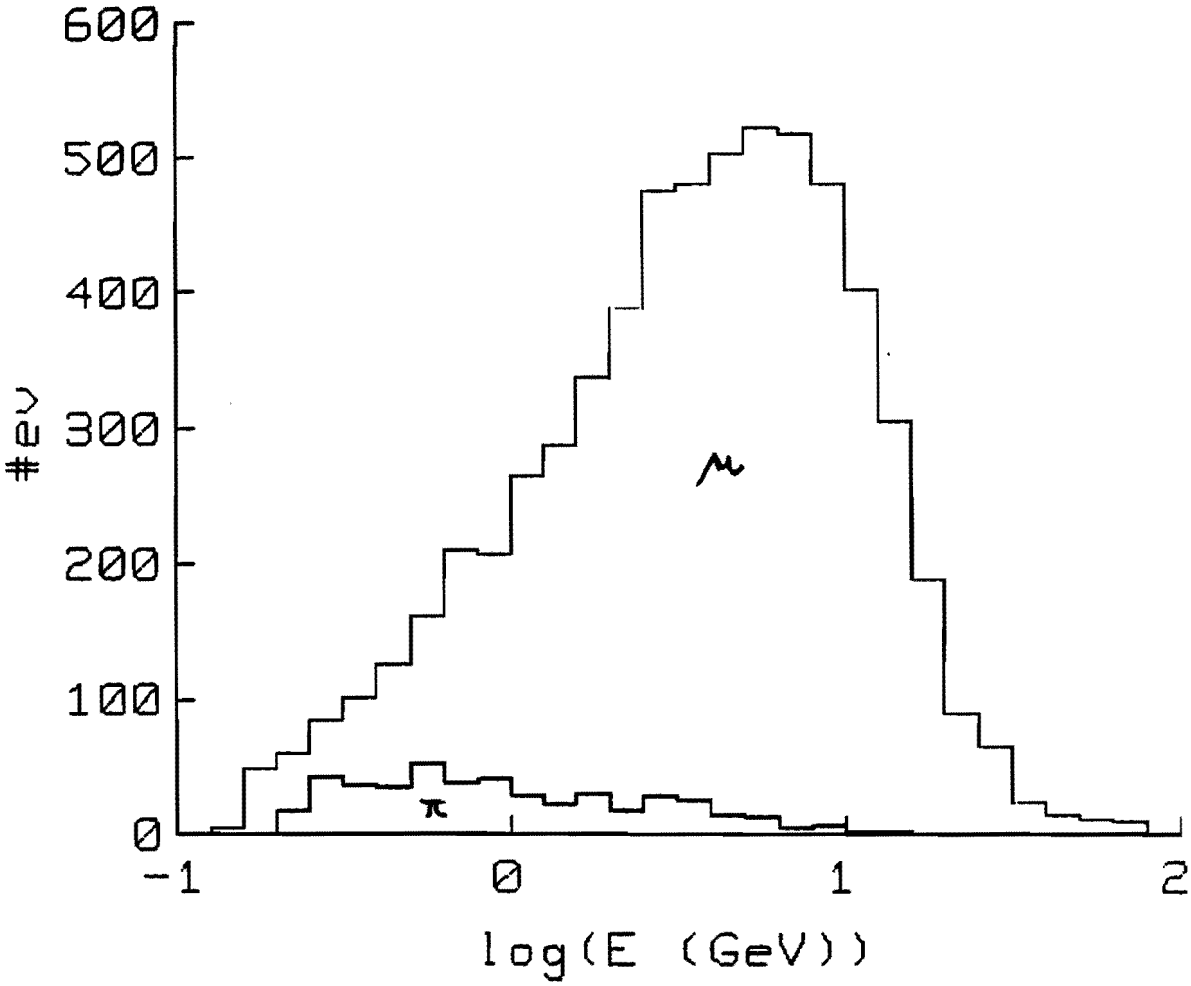

Figure 11: The energy distribution of the entering tracks.

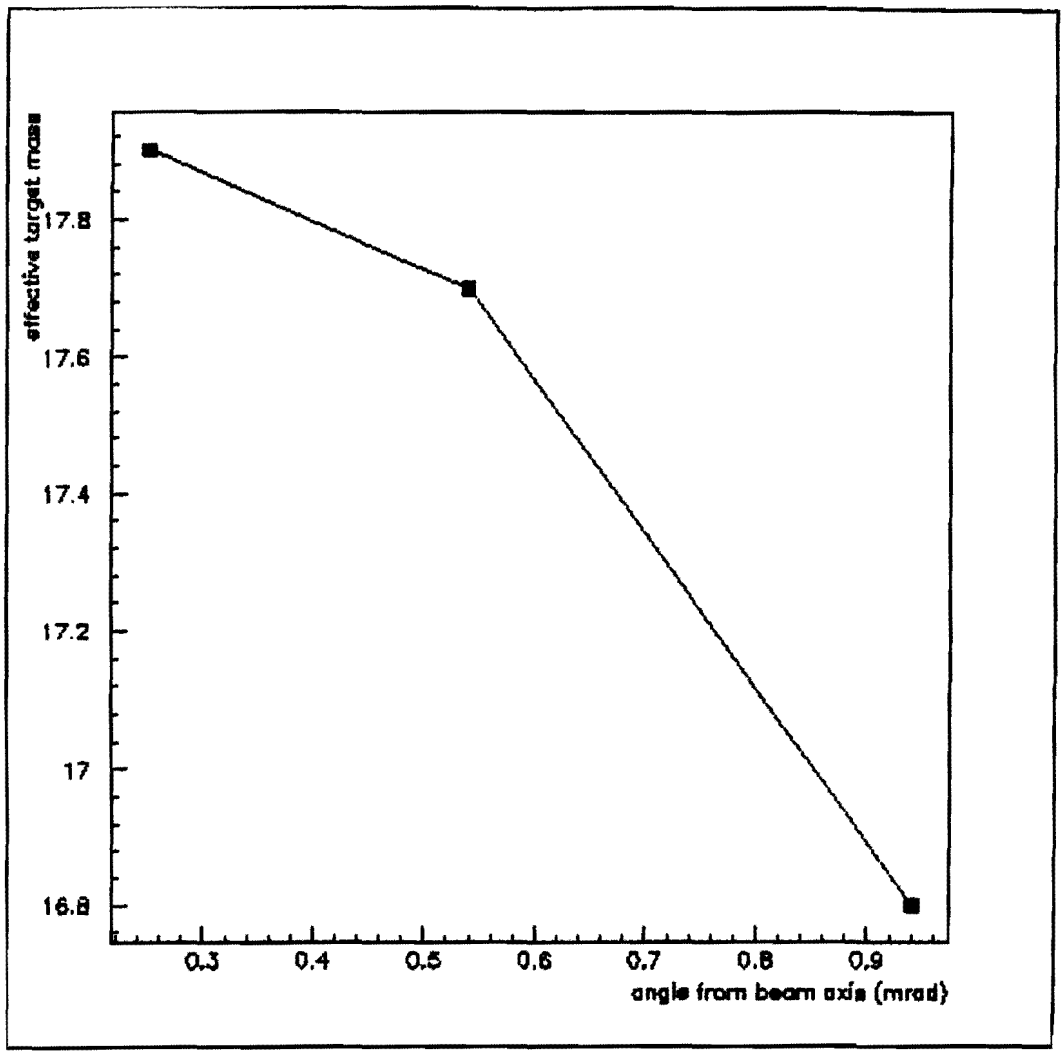

Figure 12: The total effective target mass as a function of the angle between the beam axis and the detector position.

3.1.4 The ratio of the number of muons entering the detector to the number of contained events

Let us examine closely the ratio of the number of entering muons to the number of contained events:

$$R(E) = \frac{\Phi(1 - P_\nu(E))\sigma^{cc}_{\nu_\mu} r(E)}{\Phi\sigma^{nc} + \Phi(1 - P_\nu(E))\sigma^{cc}_{\nu_\mu} + \Phi P_\nu(E)\sigma^{cc}_{\text{not}\mu}}$$

where Φ is the flux of ν_μ, and $r(E)$ is the effective target mass for neutrinos of a given energy E.

In the case of $\nu_\mu \leftrightarrow \nu_e$ oscillations the denominator measures the total flux of neutrinos, and the numerator measures the disappearance of ν_μ from the beam. In the case of $\nu_\mu \leftrightarrow \nu_\tau$ oscillations the numerator still plays the same role, while the denominator is decreased by the lower cross section of charged current ν_τ interactions. This effect diminishes the sensitivity of the experiment by as much as 59% for very low (few $\times 10^{-2}$) mixing angles and substantially cuts the sensitivity of the experiment in the region of the smallest δm^2.

3.1.5 Summary of Different Ways of Looking for Muon Neutrino Disappearance

The effect on the event rates of various manifestations of muon neutrino disappearance for different oscillation scenarios are summarized in the following table:

	$\nu_\mu \rightarrow \nu_R$	$\nu_\mu \rightarrow \nu_e$	$\nu_\mu \rightarrow \nu_\tau$
# entering muons	down $\approx P$	down $\approx P$	down $\approx P$
# contained events	down $\approx P$	unchanged	down by less than$P$
ratio	unchanged	down $\approx P$	down $\approx 0.5 \times P$

where P is the fraction of ν_μ oscillating to another flavor, so for example, if $P = 0.25$, and we have $\nu_\mu \rightarrow \nu_e$, then the rate of entering muons would be diminished by 25%.

This table might help to find the eventual predominant channel of oscillation in case some deviations from the expectations in this table are observed.

3.1.6 Estimated Oscillation Limits

If the observed signal of neutrino interactions is in agreement with the expected one, within the accuracy of our experiment, we can set limits of the mass-square difference and the mixing angle which will be different for the various oscillation scenarios. These limits are derived from the formula

$$P(\nu_\mu \rightarrow \nu_x) < \sin^2(2\theta) \int \rho(E) \sin^2\left(1.27\frac{\delta m^2 L}{E}\right) dE$$

where $\rho(E)$ is the appropriate neutrino energy spectrum and L is the oscillation distance ($L = 570$km).

When we are looking for oscillations to non-interacting neutrinos by detecting a decrease of both contained and entering event rates, then we are able to exclude a P larger than the systematic error of 0.05. The function $\rho(E)$ is the incoming neutrino energy spectrum weighted by the interaction cross-section ($\sim E$). The resulting exclusion region is shown in fig. 13.

When we are looking for oscillations by examining the ratio of the number of entering tracks to the number of contained events, we fold the results on P with the expression

$$R = \frac{(1-P)\sigma_\mu^{cc}}{0.3\sigma_\mu^{cc} + (1-P)\sigma_\mu^{cc} + P\sigma_x^{cc}}$$

To compute the P in the numerator of this expression, the spectrum $\rho(E)$ used is that for neutrinos producing entering tracks, while in the denominator that for the contained events is used. For the entering tracks this spectrum is a little harder than the $\rho(E)$ for contained events. This can be seen in fig. 14.

Due to the difference in the charged current cross-sections between electron and tau neutrinos, the limits which we can put will be different for $\nu_\mu \rightarrow \nu_e$ and $\nu_\mu \rightarrow \nu_\tau$. Assuming that we do not detect a difference between the expected and the measured ratios greater than 2%, we calculate the limits for $\nu_\mu \rightarrow \nu_e$ (see fig. 15) and for $\nu_\mu \rightarrow \nu_\tau$ (see fig. 16). Note that our experiment is slightly less sensitive for $\nu_\mu \rightarrow \nu_\tau$ oscillations but still is able to cover the region of major interest described in the introduction of this proposal.

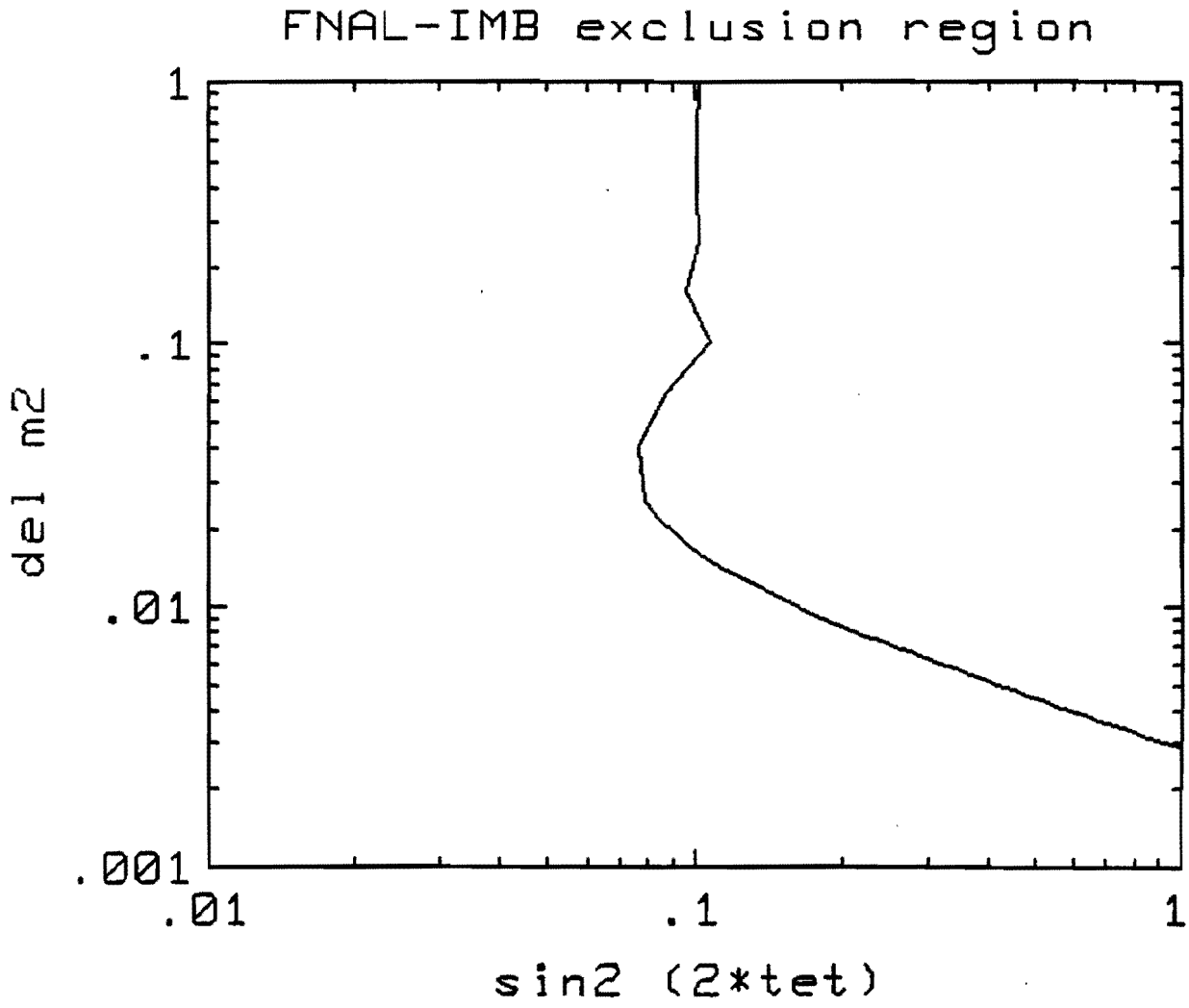

Figure 13: The $\delta m^2 - \sin^2(2\theta)$ exclusion region for ν_μ disappearance to ν_R.

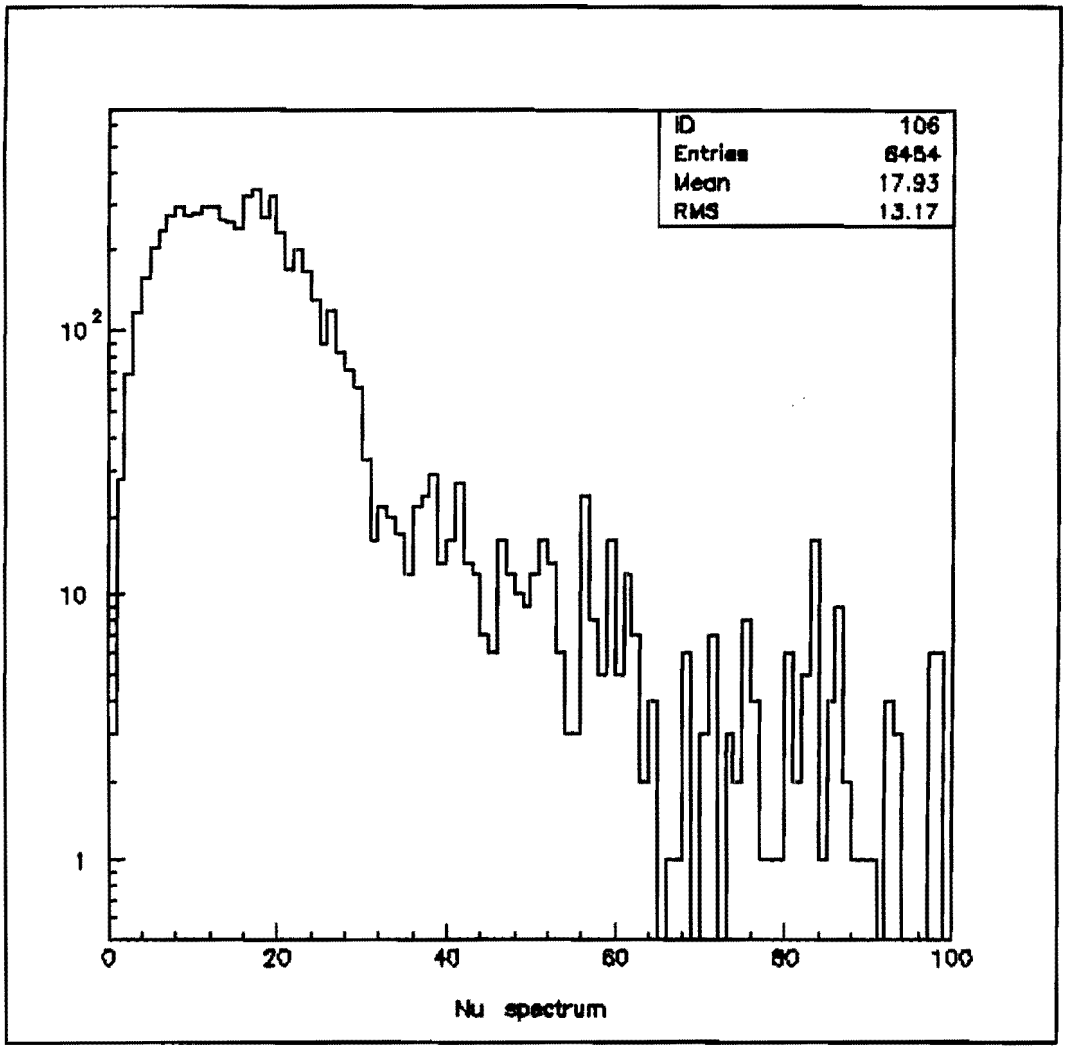

Figure 14: Spectrum of neutrinos producing entering tracks.

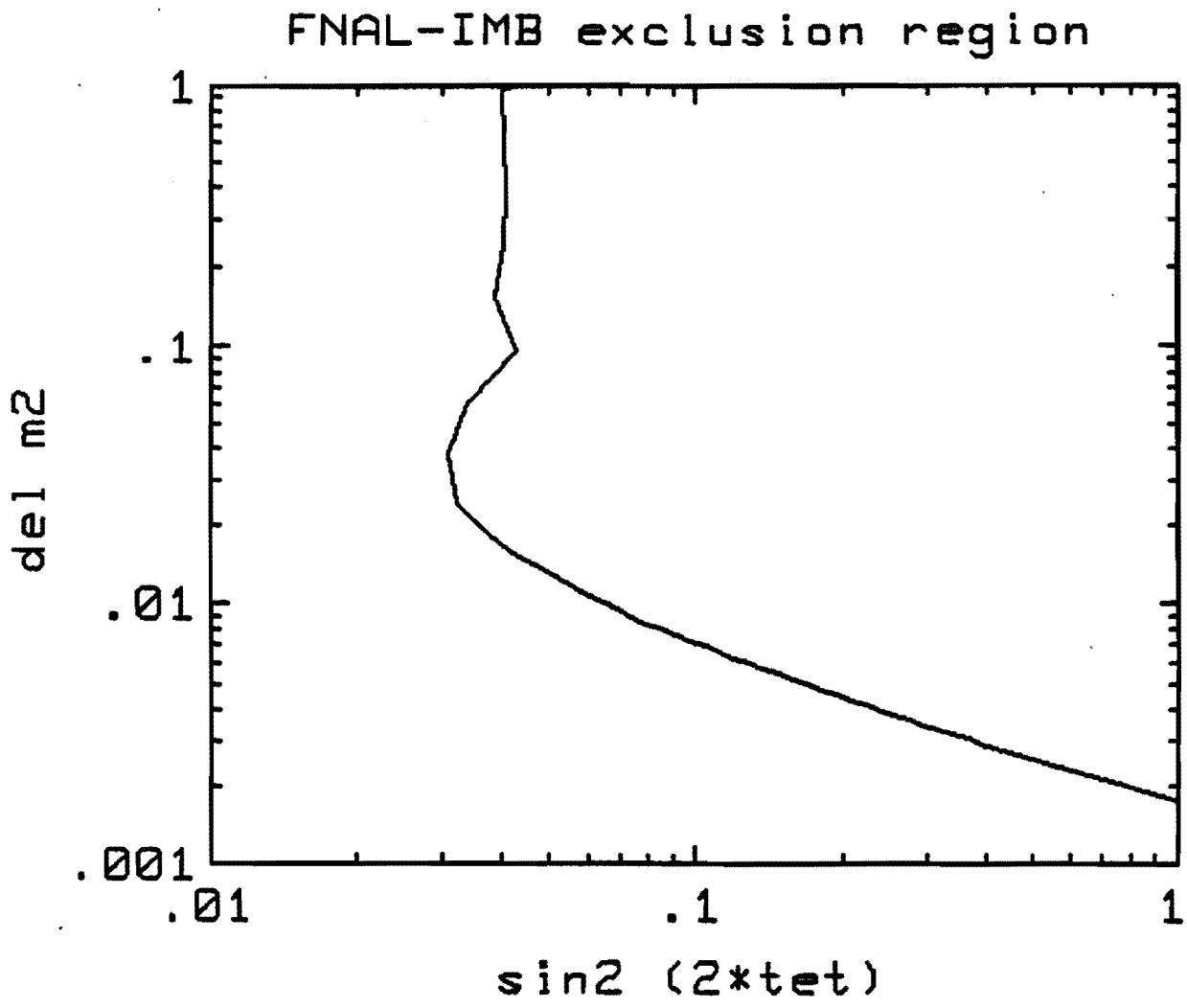

Figure 15: The $\delta m^2 - \sin^2(2\theta)$ exclusion region for ν_μ disappearance to ν_e.

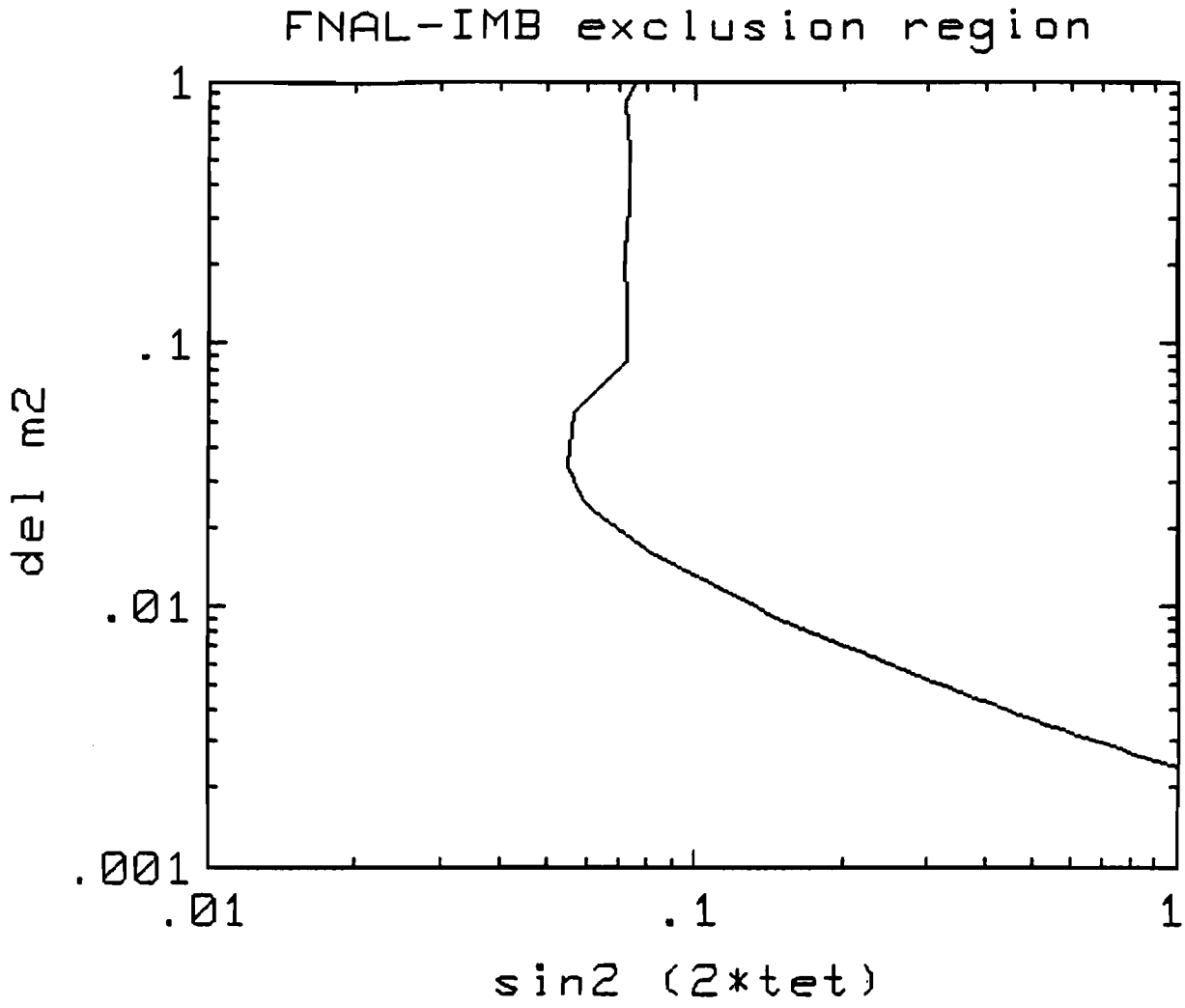

Figure 16: The $\delta m^2 - \sin^2(2\theta)$ exclusion region for ν_μ disappearance to ν_τ.

3.2 Content of Muon Tracks in the Sample of Contained Events

We are able to identify tracks as showering or nonshowering only if the track stops in the detector. Such particles are produced mainly by low energy neutrinos. The sample will consist predominantly of quasi-elastic and single pion production charged current interactions with a small admixture of neutral current events. Although the low energy neutrino spectrum is difficult to predict, an experiment of the precision of 10-20% should be possible. This sample is small but collected automatically with all the other events. Even with low precision, this kind of analysis can expand the sensitivity of the experiment to lower δm^2.

3.3 Search for Appearance of Other Neutrinos

3.3.1 Electron Neutrino Appearance

If muon neutrinos oscillate to electron neutrinos, one should observe more charged current contained interactions with electron tracks than expected from background and beam composition. The energy spectrum of these electrons should be the same as that of muons from similar contained interactions and is shown in fig. 17

The main background to showering electron tracks is due to showering tracks from π^0's produced with similar energy spectrum in charged and neutral current neutrino interactions. The spectrum of π^0 is also shown in fig. 17. One can see that leptons have a much harder spectrum than the pions. Above 10 GeV there is still about 22% of the entire leptonic spectrum, while the π^0 background is only 5% in this energy region.

The contamination of the ν_μ beam by electron neutrinos in the higher energy part of the spectrum is expected to be less than 1%.

These conditions are summarized in the following table:

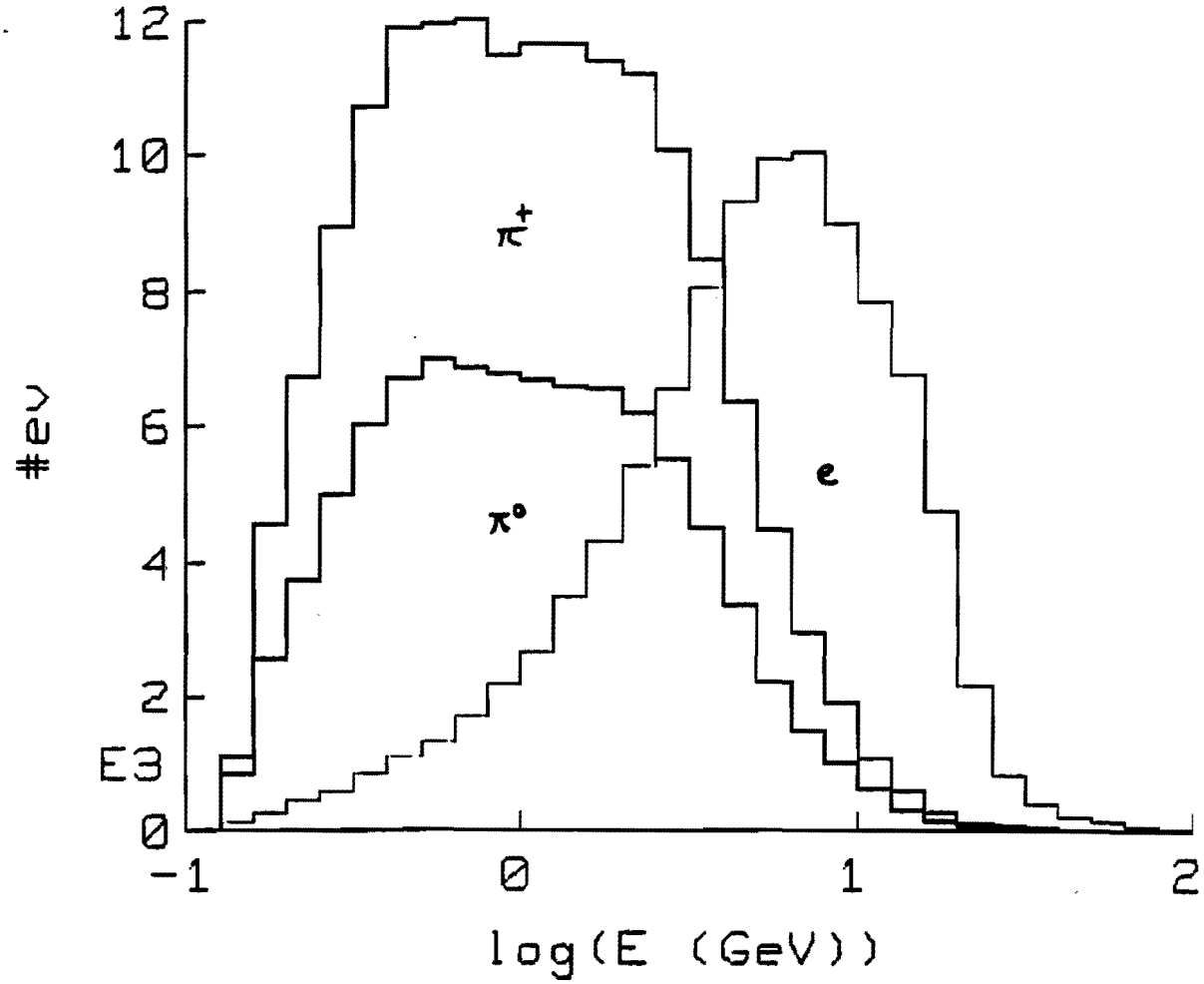

Figure 17: The spectrum of electrons from contained charged current interactions

Total leptons collected in one half year	5400
Leptons with$E > 10$GeV	1185
$\pi^0$with$E > 10$GeV	59
$\nu_e$contamination	12
total background	71
90%confidence limit	82

The spectrum of neutrinos producing leptons of energy higher than 10 GeV is shown in fig. 18.

If one does not observe more than the predicted background of 71 showering tracks in a half year of data collection, one can set limits on the δm^2 and mixing angle as shown in fig. 19

One must notice that the precision with which the electron appearance can be observed is already of the order of 1% after a half year of data collection. Due to uncertainties in calculating the backgrounds from high energy π^0 and the ν_e contamination of the beam, a more precise search for ν_e appearance can not be made.

3.3.2 Tau Neutrino Appearance

It is extremely important to be able to search for a signal of tau neutrino appearance. A possible signature of such a process could be an excess of electron tracks from tau meson decays in the contained sample. However, such a signal is completely hidden by π^0 tracks, as shown in fig. 20, making its demonstration questionable.

Nonetheless, if we can demonstrate muon neutrino disappearance, and if we do not observe sufficient excess of high energy electron tracks, tau neutrinos would be the most natural channel to which the oscillation could take place.

Because of the importance of a positive detection, we shall continue to pursue studies attempting to find a mode which could positively identify tau decay.

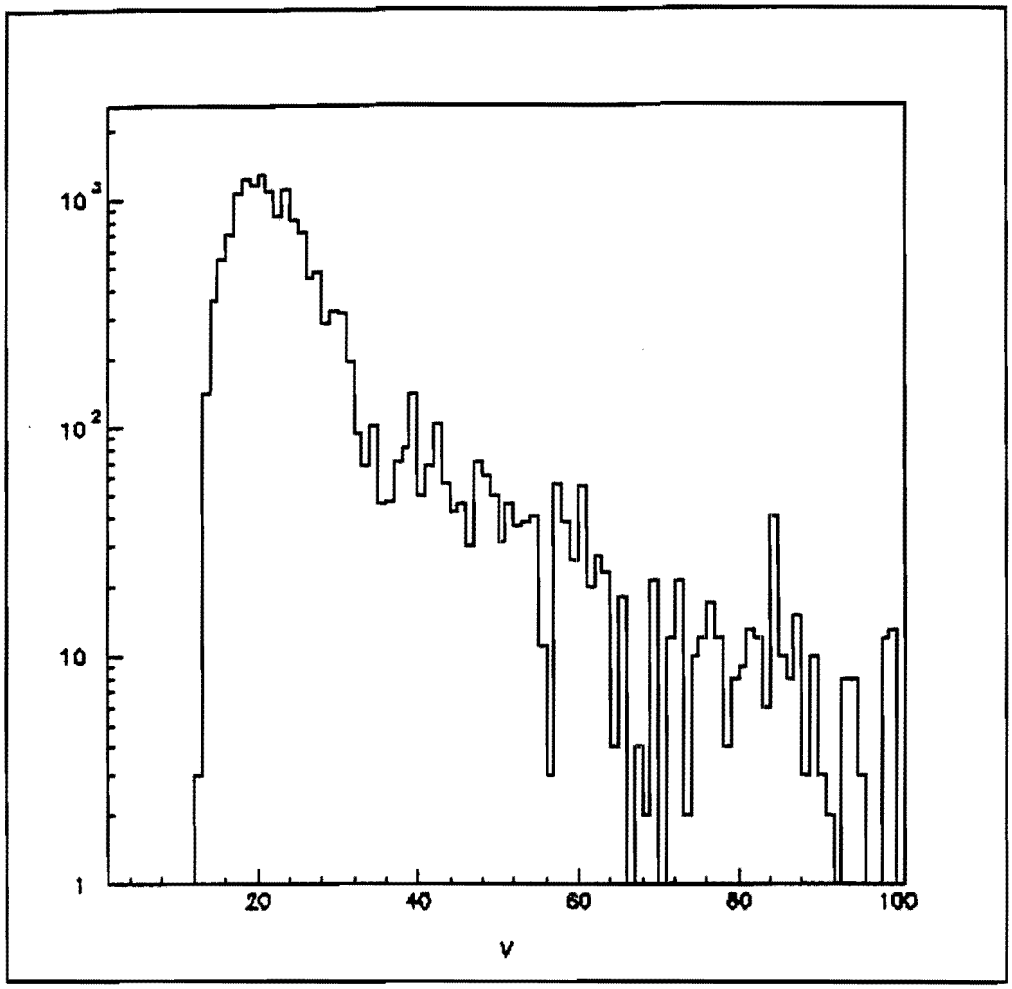

Figure 18: The spectrum of neutrinos producing leptons with energies higher than 10 GeV.

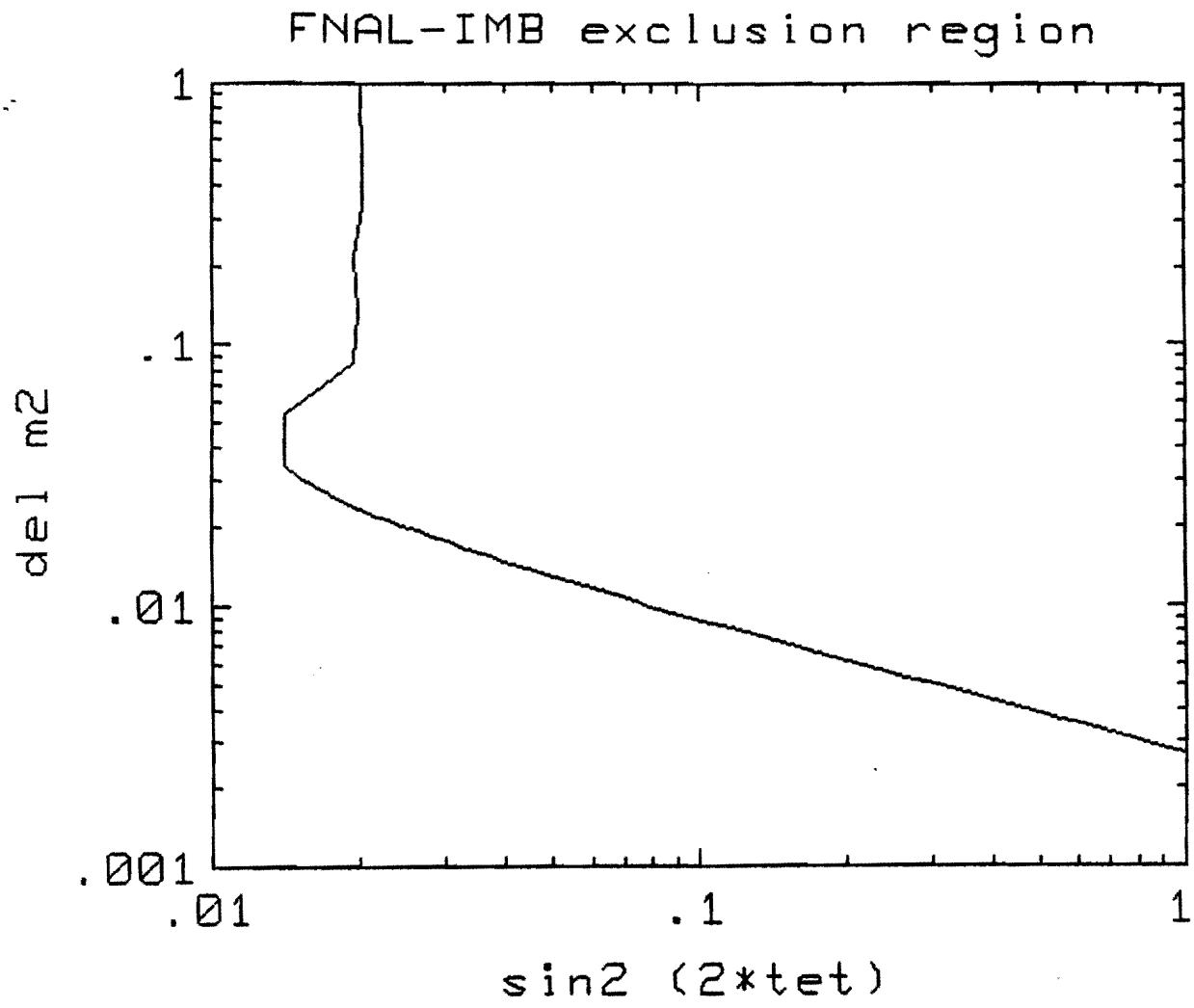

Figure 19: The $\delta m^2 - \sin^2(2\theta)$ exclusion region for $\nu_\mu \rightarrow \nu_e$ appearance.

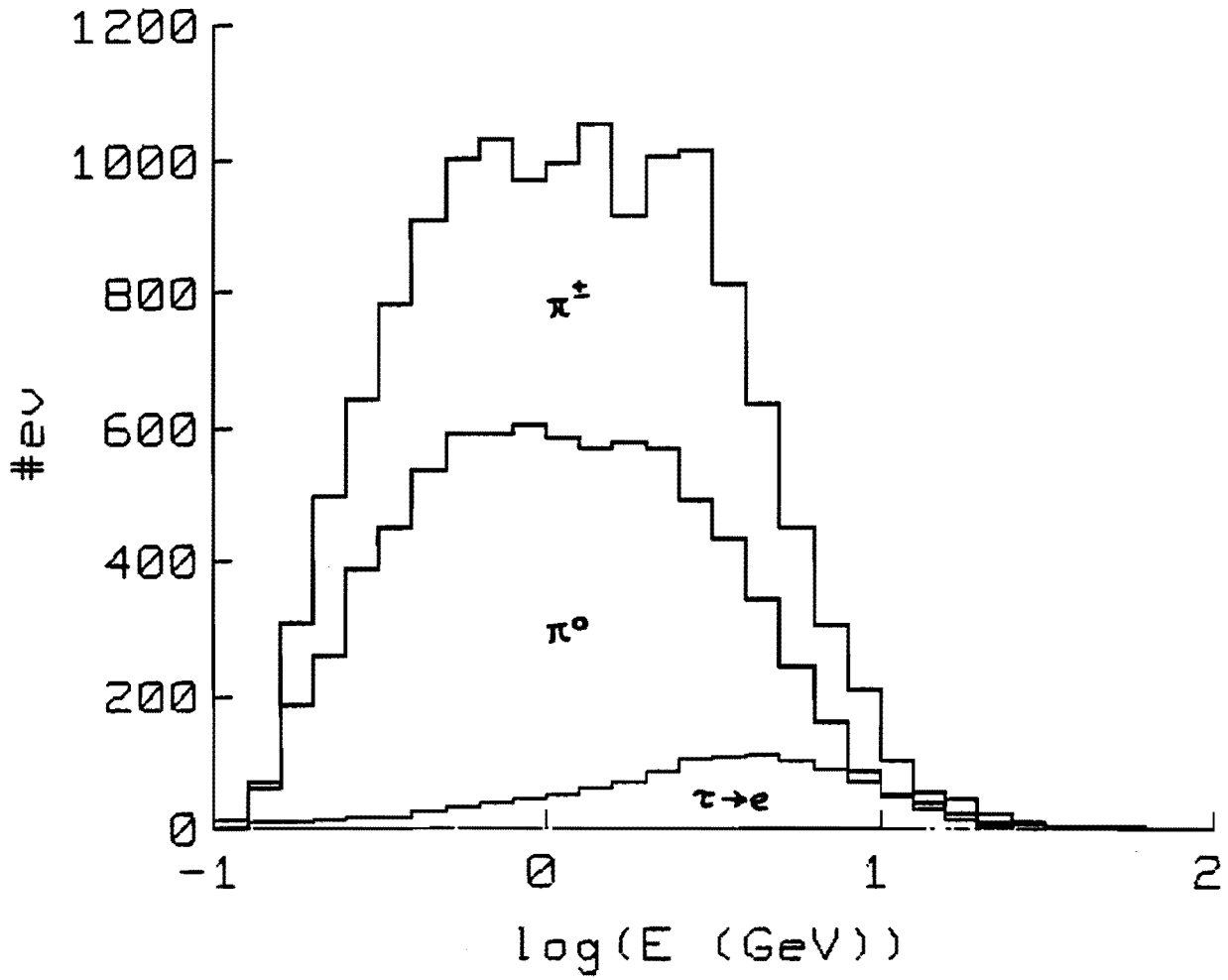

Figure 20: Comparison of the energy spectrum of electrons from τ-lepton decay with the energy spectrum of π^{o} produced in deep inelastic ν_{τ} interactions.

4 Cost of the Experiment

As has been stated, only minimal changes will be required in the existing detector. Necessary changes include improving the definition of the fiducial volume of the detector. These changes will be made within the regular maintenance funds provided by the DOE. However, FNAL must provide the beam, the costing of which is discussed in the "Report of the Research Division."

We require additional equipment to record the time of every proton beam spill producing neutrinos in the direction of the IMB detector. In addition to signals regularly provided we need:

1. GEO clock	4850
2. CAMAC and controller	3500
3. Clock to CAMAC converter	1300
4. Computer to read CAMAC, preferably a MicroVAX	8400
5. Tape drives and SCSI interface to record data	2800
	20,850

A Beam Design

The neutrino beam line is the only element of the proposed experiment which has to be constructed. It is important that the beam line has facilities to accommodate an additional neutrino experiment situated close to the end of the decay pipe (short baseline experiment).

The extraction of the proton beam from the Main Injector in the right direction (East) does not contribute any special problems as there is a straight section of the main ring which can be used for this purpose. There is also sufficient space between the Main Injector and Tevatron rings to accommodate the proposed beam line. The primary requirement is excavation of a trench going downward with the proper angle ($\approx$ 45 mrad), in which the beam line can be constructed together with facilities for the short base line experiment P803. The technical implementation of this scheme is described in the Conceptual Design Report from the Research Division of FNAL. The considered layout of the beam line is shown in fig. 21 What we need to stress here is that the construction of the proposed beam line should be strongly coupled with the construction of the ring for the Main Injector.

The active elements of the neutrino beam, which we propose to construct, have been designed on the basis of the broad experience collected over the years at FNAL and CERN. The main requirements to their design include:

1. Full utilization of the capacity of the Main Injector.
   - proton beam intensity up to 4×10^{13} ppp.
   - proton energy of 120 GeV.
   - short cycle time of 1.5–2.0 sec.
   - intermediate spill time of about 1.0 ms.
2. The resulting neutrino flux has to provide a reasonable signal in the IMB detector of at least two interactions in the detector volume per hour.
3. Compatibility of the neutrino beam characteristics with the requirements of the P803 experiment.

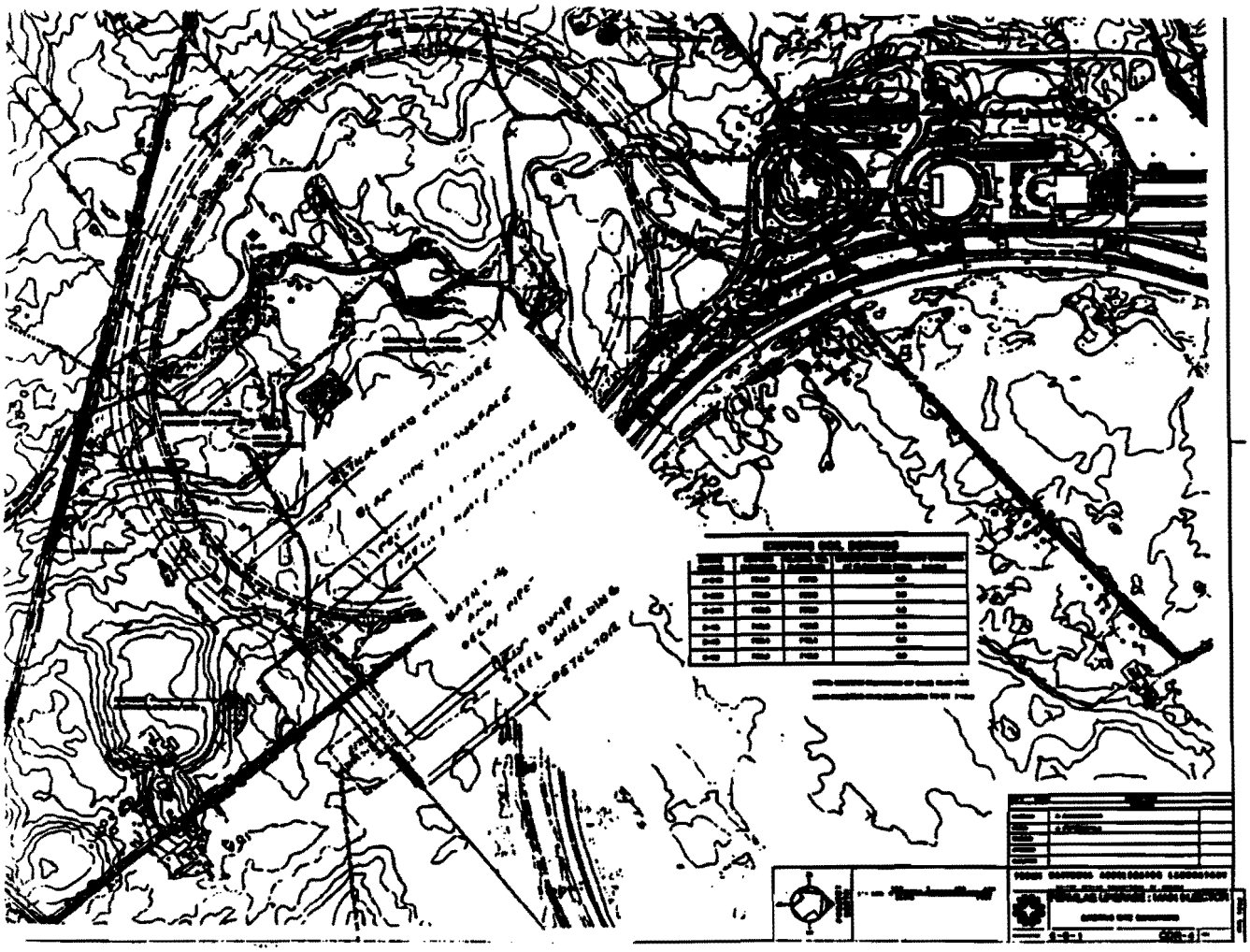

Figure 21: Proposed layout of the neutrino beam line.

4. Reasonable cost of the beam line, which means using a short length decay pipe while still providing the required flux.

We describe here only the most complex elements of the beam line and argue that they can be constructed. These elements are:

1. target
2. horn focusing system
3. decay pipe

A.1 The Target

Experience at CERN [8][9] indicates that a traditional target material, beryllium, cannot withstand the intensity of the beam from the Main Injector. The only material which can survive such conditions is graphite. In addition the use of a series of slim target segments (diameter 3–6 mm), rather than one solid bar of one interaction length, increases the output of secondaries. We propose a target consisting of 11 graphite rods each 6 mm in diameter, 10 cm long and separated by 9 cm. The total length of such a target is 2 m. The individual rods are supported from the sides by 1 mm thick graphite plates.

We have not been able so far to get a good estimate of the energy deposited by the primary beam in the graphite target. Various programs give results different by a factor of 5, and the standard program FLUKA used for this purpose at CERN is not available. We are going to work along the lines shown in reference [10] to design the target and its cooling system. The results will be presented in the forthcoming Conceptual Design Report of the FNAL Research Division.

A.2 The Horn System

Existing horn designs are optimized for focusing either a selected interval of energy or momentum transfer. Our purposes are best served by the latter which provides more efficient focusing over a broader range of particle momenta. In addition the horn system is optimized for an extended target of length 2 m.

The system, which has been designed by A. Malensek and which we are prepared to implement, is shown in fig. 22. It consists of two units separated by 16 meters. The length of each unit is about 4 m, which is dictated by machining constraints of the inner conductor. It has been CERN's experience [11] that welded inner conductors in horns cannot withstand the pulsing magnetic pressures, which are on the order of 1 ton/cm^2, produced by horn currents of 100–200 kA. The shape of the inner conductor of each unit has been chosen in such a way that the integral of

$$0.03 \int Bdl = p_t \approx 500\text{MeV}/c$$

over the particle trajectory through the horn system. The magnetic field in the horn is: $B = 0.2I/r$ in kilo-Gauss, I is in kilo-amps, and r is in cm. A simple program calculating beam trajectories using the Runge-Kunta method through the magnetic field of the horns was applied. The program also calculates the efficiency for collecting secondaries in a cone of 2 mrad for one of the models of hadron production in the target. Fig. 23 shows the efficiency for the outer-most, central and inner-most parts of the target, in its optimal position with respect to the horns.

In order to obtain the final optimal current for this horn system the GBEAM program described in Appendix B has been run with various values of the horn current. In fig. 24 the total flux of neutrinos in a cone of 1 mrad is shown as a function of the current. The plot indicates that the optimal current is 160 kilo-amps and that a variation of the neutrino flux of the order of 10% per 10 kA is expected.

The GBEAM program indicates that interactions of secondaries, mainly in the aluminum of the horn system, cause a decrease of the final neutrino beam flux by as much as 30%. Fig 25 shows the comparison of the spectra of positive pions entering the decay tunnel for a beam line with and without the material of the horn conductors. One can see, that the re-interactions lead to a decrease of the flux and a softening of the pion energy spectrum. In addition, as is illustrated in fig. 26, the angular distribution of secondaries entering the decay tunnel gets wider due to such re-interactions, causing more of them to hit the walls before they decay.

These simple considerations illustrate the need for further optimization of the thicknesses of the horn conductors. An applicable method [12] con-

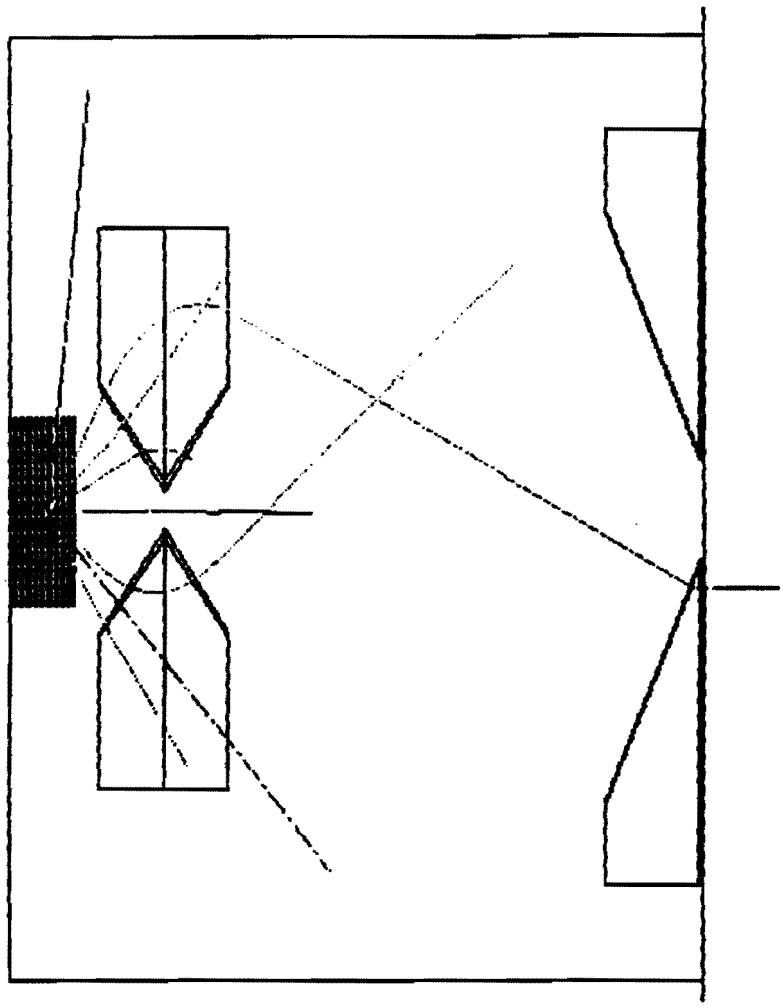

Figure 22: The horn system.

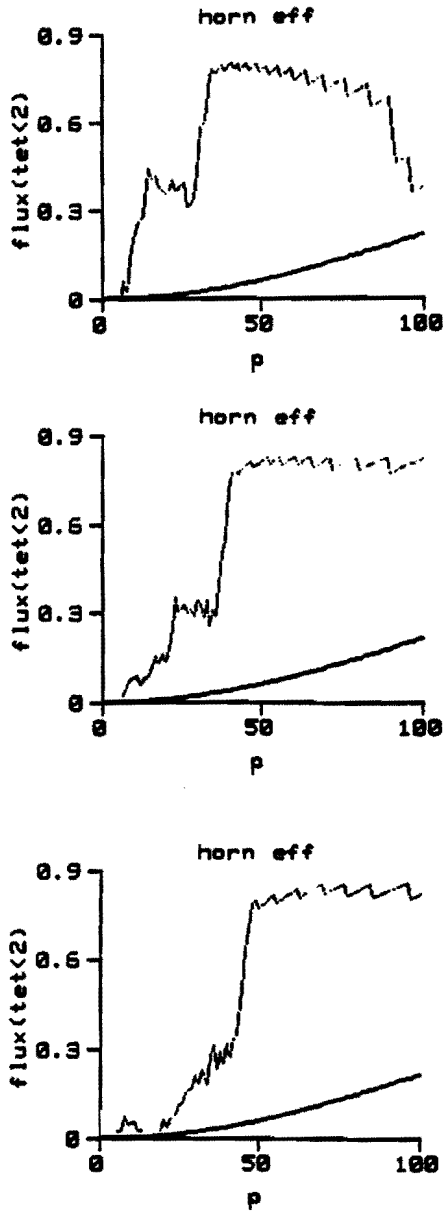

Figure 23: Efficiency of the horn for various parts of the target. Top: portion of target closest to the horn. Middle: central portion of the target. Bottom: portion of the targest furthest from the horn.

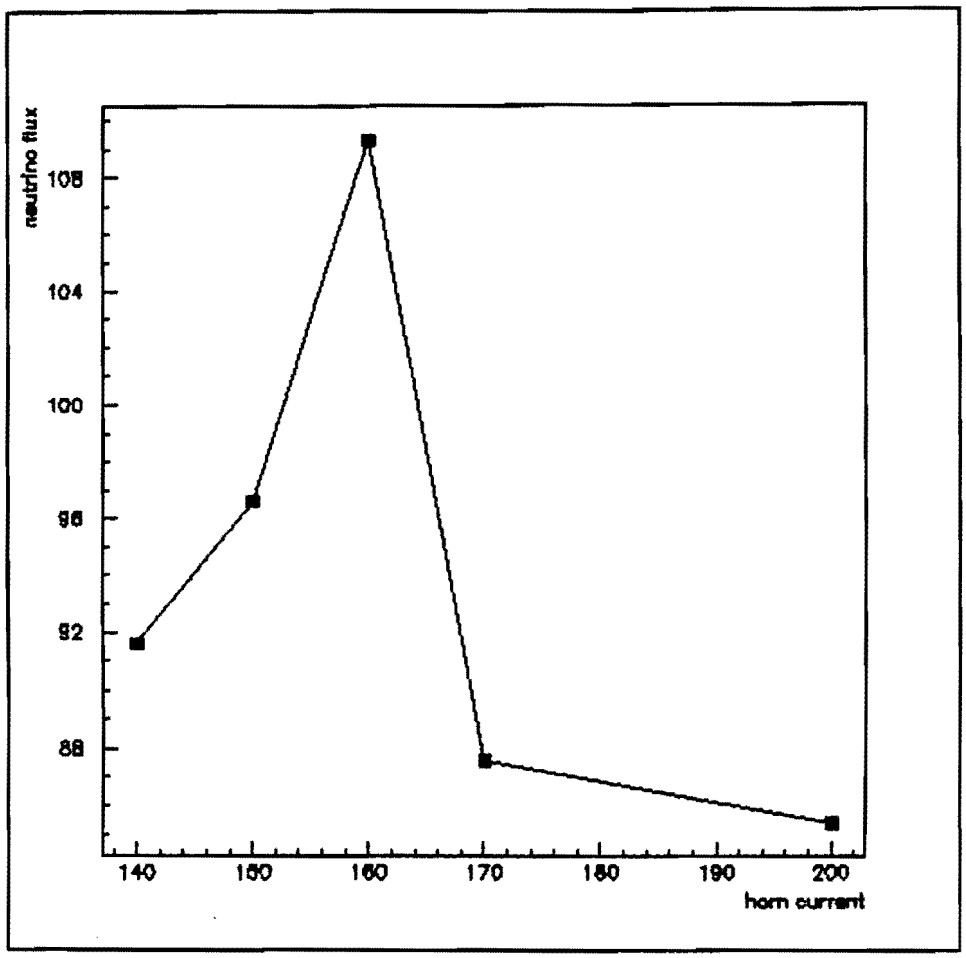

Figure 24: Neutrino flux versus horn current.

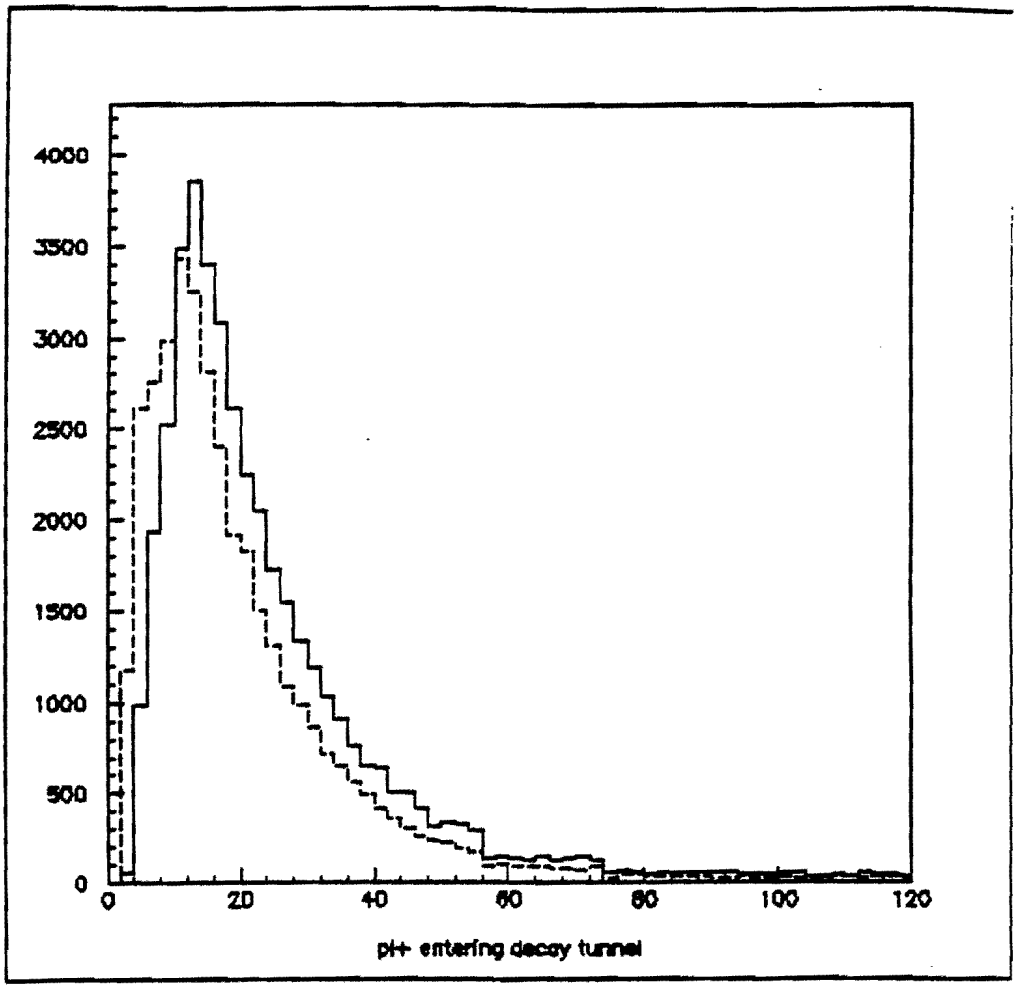

Figure 25: Spectra of π^+'s entering decay tunnel with (broken line), and without (solid line) the horn conductor matter.

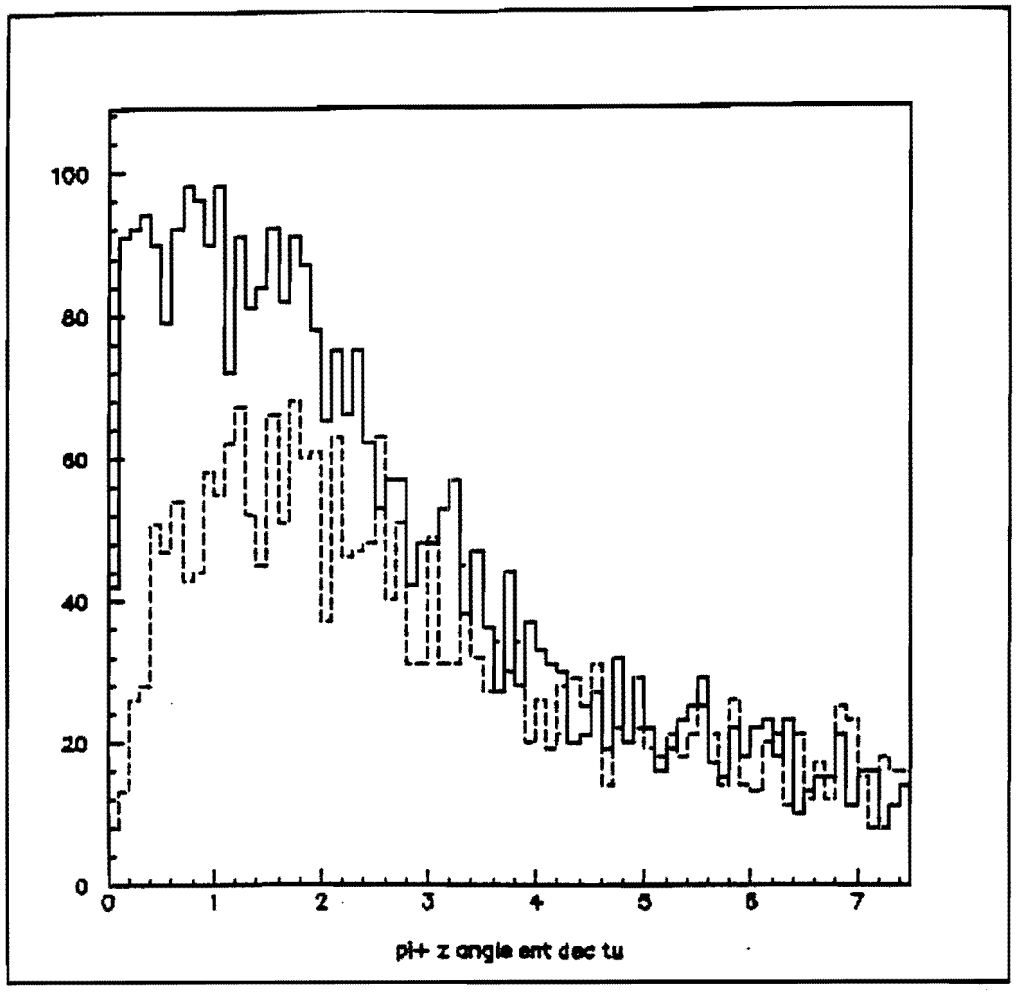

Figure 26: π^+ entering decay tunnel with (broken line), and without (solid line) the horn conductor matter.

sists of solving the equation of motion of the conducting matter under the magnetic pressure generated by the pulsing current. Obtained in this way stresses of the conductor walls cannot exceed the material strength. The final thicknesses of the horn conductors must be a compromise between the results of such calculations and limitations due to machining of the conductor. So far we use the results of this method with a wide safety factor. Further detailed research and development of the horn design can improve the final neutrino flux by as much as 10–20%.

A.3 Decay Tunnel

The flux of neutrinos produced by the beam line is proportional to the length of the decay tunnel in the range of a few hundred meters. Also a longer decay tunnel enriches the higher energy part of the neutrino spectrum; however, the decay tunnel, constructed using an evacuated steel pipe 1–1.5 m in diameter, is the most expensive part of the beam line. The cost is mainly due to radiation environmental protection requirements. Also the fact that the decay tunnel must point underground at an angle of 45 mrad escalates this cost.

Our beam design strives to minimize cost while maintaining a suitable flux of neutrinos. We chose a short (300 m) decay pipe, compensated by an efficient target and horn system. To decrease to construction cost of the beam line, we propose to apply the so called "roller coaster" scheme. The decay pipe and its insulation to protect the ground water, will be situated in an excavated trench. To decrease the depth and the cost of the excavation we use the dirt from the trench to build a hill. The extracted proton beam will be bent to the top of the hill and then down again towards IMB. The target and horn area (25 meters in length) will be put close to the top of the hill.

B Neutrino Beam Monte Carlo

We have adopted a program, GBEAM, used by the CHARM collaboration at CERN to calculate the neutrino output of the beam line described in Appendix A.

The program GBEAM [13] is based on GEANT to follow particles through matter and magnetic fields. In this particular application, particle decay routines have been modified to introduce distinctions between different neutrino species. The package TATINA was used to generate the hadronic interactions. The author of that program did not observe particular differences between the various hadronic packages TATINA, GHEISHA and FLUKA in the neutrino output [14].

For better precision than provided by TATINA, interactions of protons with energy above 20 GeV in the graphite target are handled by a routine based on the model described in Appendix C.

Both primary protons and the secondaries produced along the beam line are followed through the realistic setup provided to the program in the routine UGEOM. That setup, drawn by the interactive version of the program, is shown in fig. 27. When the particles reach the decay pipe several of their decay kinematics are generated and neutrinos produced are followed to the "detectors". This approach saves CPU time, but sometimes increases the probability of local fluctuations.

The IMB detector at the distance of 570 km has an acceptance of a few nano-sr. No Monte Carlo technique can provide a sizable signal within such an acceptance. In order to overcome this drawback, the neutrinos are collected on annuli of equal area surrounding the beam axis. The beam characteristics, the flux and the energy spectrum, are studied as a function of the angle between the beam axis and the detector. For the analysis in this proposal we assume that the IMB detector sees neutrinos with the characteristics of the innermost annulus.

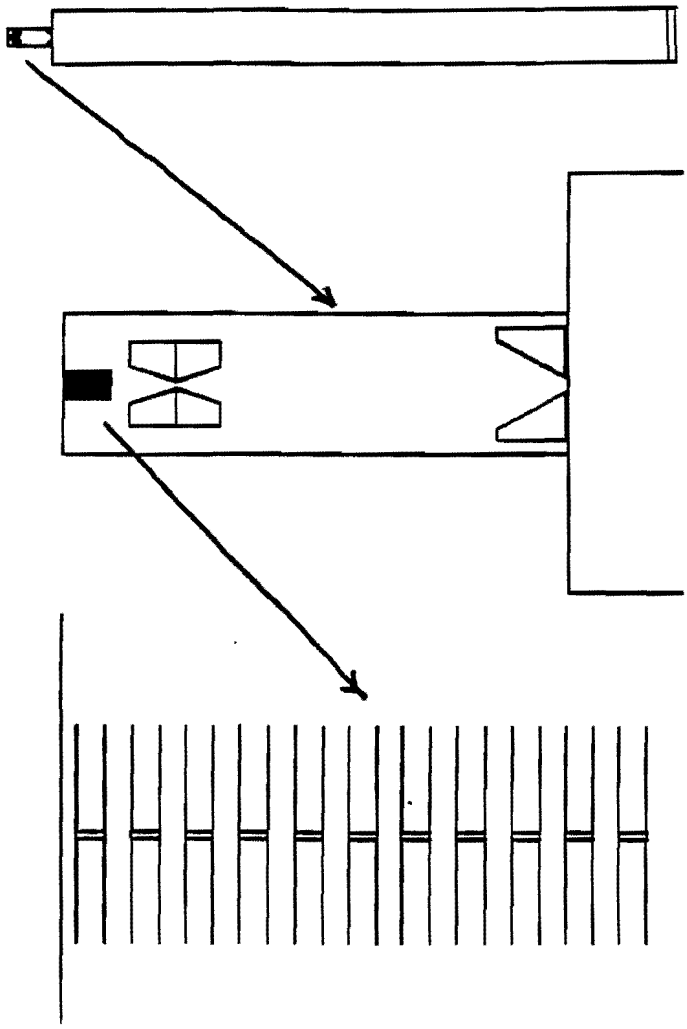

Figure 27: The beam layout as processed by the GBEAM program.

C A Model for Production of Secondaries in p–Graphite Interactions at 120 GeV

So far we have applied a phenomenological model developed by N. Stanton from the P803 collaboration to calculate the production of $\pi^{\pm}$, $K^{\pm}$, and K^0_L in $p + C$ interactions. For production of $\bar{p}$ and secondary protons we used the model of ref. [15] as implemented in the original GBEAM program.

All of these models have their parameters fitted to the measurements of inclusive cross sections from the following papers:

- for $p + p$ interactions at 100 and 175 GeV: ref. [16].
- for $p + A$ where A is C, Al, Cu, Ag, or Pb at 100 GeV: ref. [17].

C.1 The Model for $\pi^{\pm}$, $K^{\pm}$, and K^0_L Production

The invariant inclusive cross sections have ben parameterized in the following form:

$$\left(E\frac{d^3\sigma}{dp^3}\right) = \left(C\,(1-x)^{Nh} + a\right)\left(e^{-bp_t}\right)$$

The parameter x has been defined as $x = \frac{2E^{CMS}}{\sqrt{S}}$ where the center of mass is the p–p system, $\sqrt{S}$ is the total center of mass energy of the system. The parameters C, a, Nh and b were taken from Reference [16] and are listed in the table. One has to notice that the available data in Reference [16] covers a range of $0.2 \leq x < 1$ and $0.25 < p_t < 1.25$ GeV/c.

The invariant cross sections on nuclei have been fitted introducing corrections to the x dependence, p_t distributions were assumed to be as for the p-p interactions (no available data).

$$\left(E\frac{d^3\sigma}{dp^3}\right)_{pN} = \left(E\frac{d^3\sigma}{dp^3}\right)_{pp} D\,(1-x)^{Nn}\,A^{\alpha(x)}$$

The factor $A^{\alpha(x)}$ (A being the mass number of the nucleus) has been fitted in Ref. [17] to the form $\alpha(x) = 0.74 - 0.55x + 0.26x^2$. Our values for D and Nn are listed in table 1. The agreement of these fits with the available data is illustrated in the figure 28. Note the magnitude of the uncertainties of the

	π^+	π^-	K^+	K^-
C	18.68	11.89	1.50	1.32
N_h	3.47	4.37	2.73	5.42
b	4.08	0.010	0.	0.
D	1.39	2.25	1.88	2.09
N_n	−0.485	0.34	−0.40	0.0
Multiplicity $x > 0.04$	1.32	1.27	0.19	0.16

Table 1: List of parameters used in the model for $\pi^{\pm}K^{\pm}$ production in $p+C$ interactions.

measured cross sections is at best 3% and typically 10% for π^+ production, 10–20% for K^+ production. Also the measurements only span the range of $x > 0.3$.

The multiplicities for every particle produced are given by the formula:

$$dN = \frac{1}{\sigma_{in}} \left(E \frac{d^3\sigma}{dp^3} \right)_{pN} \frac{1}{x} dx p_t dp_t$$

where σ_{in} is a total inelastic cross section. We have obtained the values of these cross sections from the compilation of the world data available in the routine GMSIGM of GEANT. The same total cross sections are used by GEANT to calculate the interaction length in the target, so their values cancel and, effectively, the measured inclusive cross sections are used in this scheme.

Also note that the multiplicity is rising hyperbolically with decreasing x. The behavior of the inclusive cross section at smaller x is known neither from experiment nor theory. Most neutrinos are produced in decays of 40 GeV π^+ ($x > 0.33$); however, the low energy part of the neutrino spectrum is due to pions of smaller values of x.

In our implementation we have used the x and p_t distributions given by the above formulae as universal, independent of the energy of the primary particle. We generate only particles with $x > 0.04$. The number of each type of particle produced per interaction has been obtained from integration

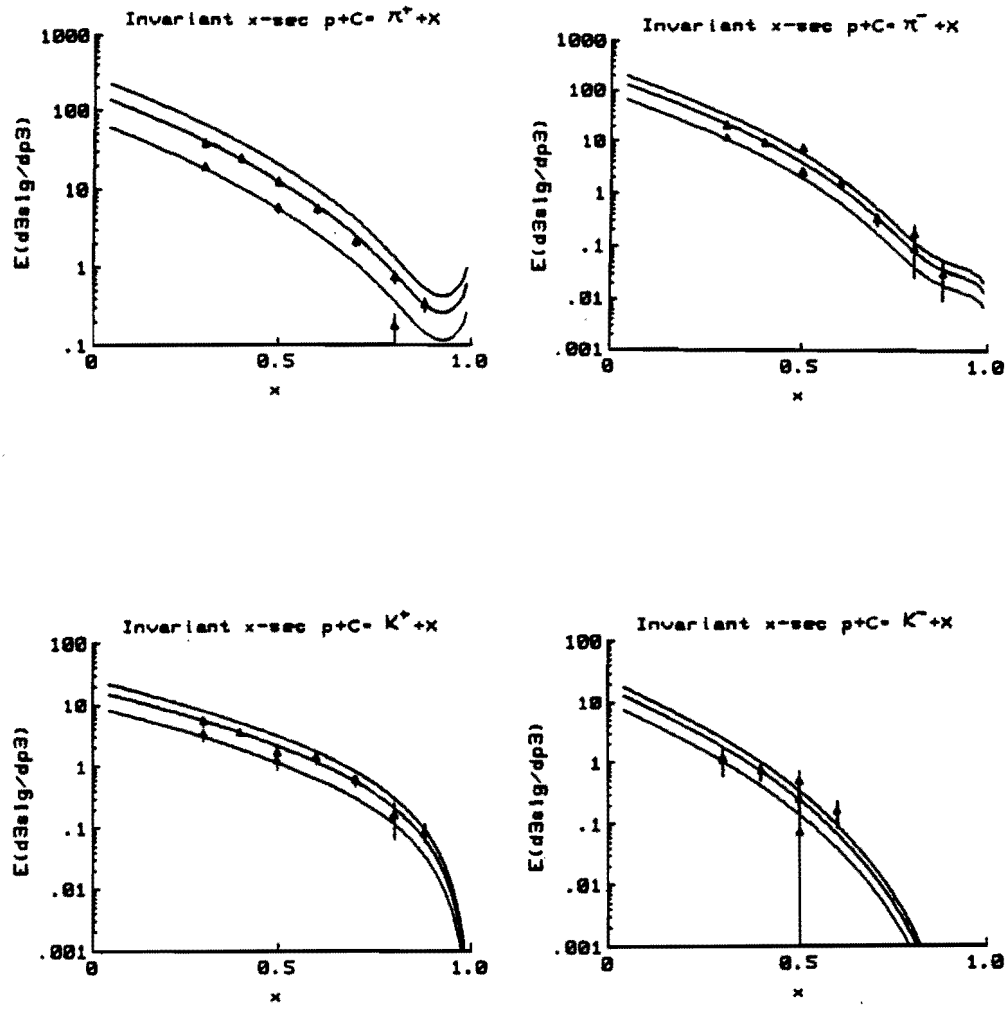

Figure 28: Comparison of various inclusive cross sections measured for $p+C$ interactions with fits used in the described phenomenological model.

of the above formulas

$$N = \int_{0.04}^{1} dx \int_{0}^{\infty} dp_t dN.$$

and is listed in table 1

It has to be stressed that, with the available data for p-C interactions, this model has a predictive power of the accuracy of the measured cross sections for the neutrinos from decays of higher energy π and K and is only an estimate for low energy neutrinos.

C.2 Model for Antiproton Production

Since we are interested in the antiproton production for momenta above 20 GeV/c ($x > 0.17$), and they do not contribute directly to the neutrino flux, we have adopted a formula from the GBEAM program. It uses

$$dN = \frac{A}{\sigma_{in}} e^{-ax} dx p_t e^{-bp_t} dp_t$$

which assumes that the invariant cross section falls to zero for $x \to 0$, instead of tending to a constant as in our model. Nevertheless the formula is fitted to the available data, providing $A = 0.02$, $a = 20.51$, $b = 3.0$, and should be reliable in the region of interest. A comparison of this fit with the available data is show in figure 29.

C.3 Model for Proton Production

For secondary protons we also consider the region of $x > 0.17$ ($p > 20$ Gev). Due to a different production mechanism a different function is used to fit the x distribution:

$$dN = \frac{A}{\sigma_{in}} x^n dx p_t e^{-bp_t} dp_t$$

giving the parameters $A = 0.49$, $n = -0.69$, $b = 3.05$. The comparison of this fit with the available data is shown in figure 30.

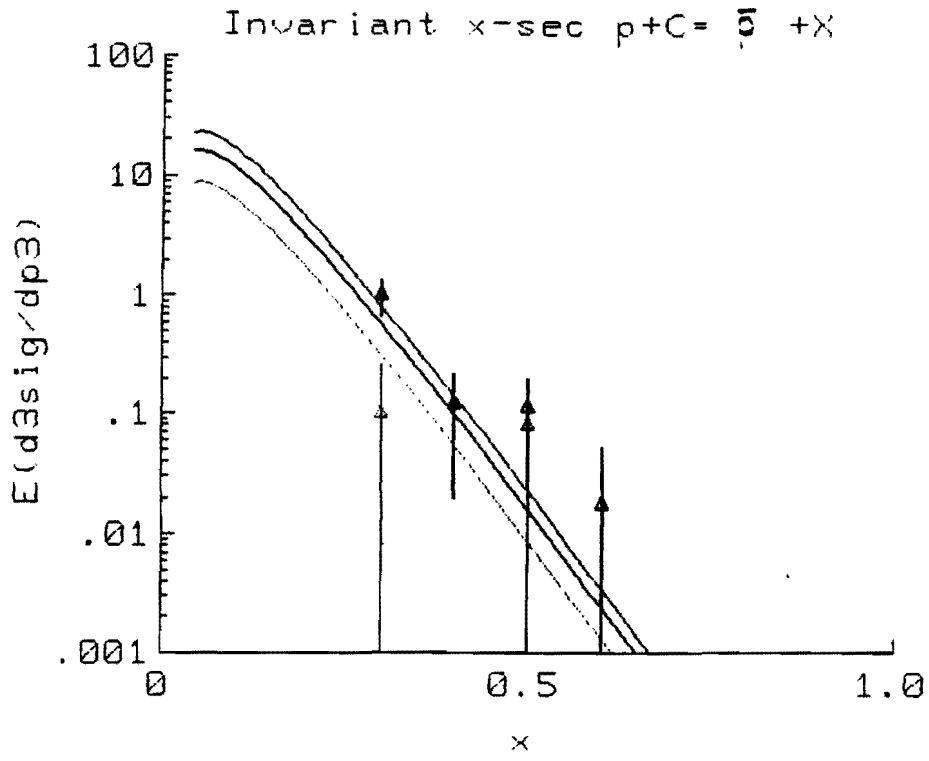

Figure 29: Comparison of measured inclusive cross sections for $p + C \rightarrow \bar{p} + X$ with fits used in our model.

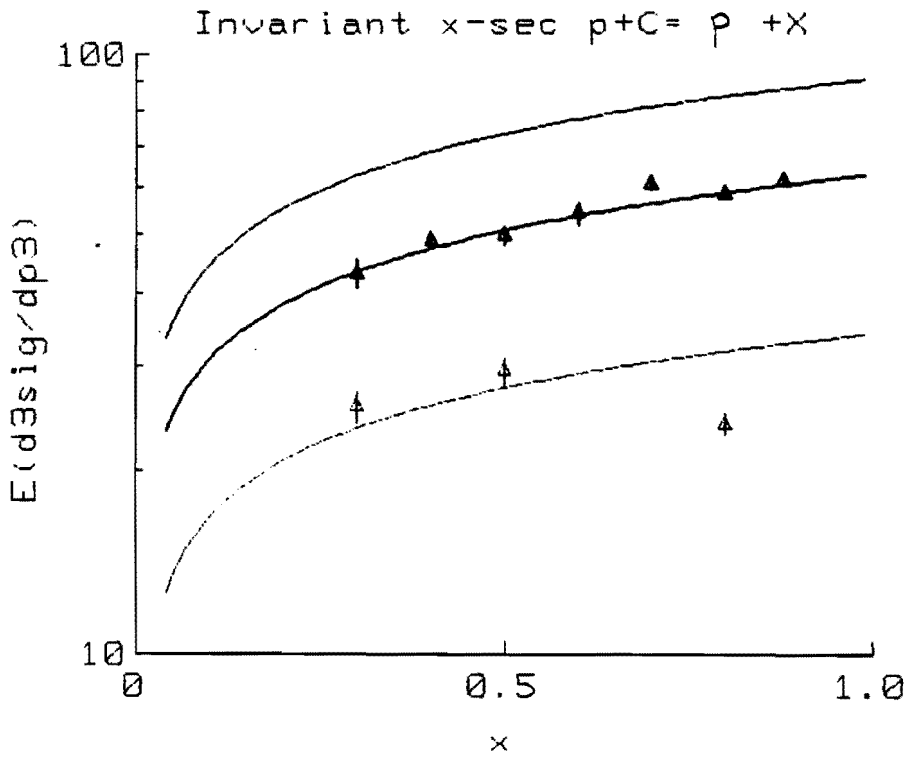

Figure 30: Comparison of measured inclusive cross sections for $p + C \rightarrow p + X$ with fits used in our model.

D Programs to calculate the signal from neutrino interactions

D.1 Deep inelastic neutrino scattering

We adopt the LUND program, LEPTO, for the calculation of particle production in charged and neutral current interactions of different kinds of neutrinos. This program generates leptonic and quark vertices according to proper y and x distributions. Structure functions for different valence and sea quarks are from fits of Gluck, Hoffmann and Reya (Z. Phys. C13, 119, (1982). When the energy transfer to the quark system, W, exceeds 2 GeV (the value setup in the JETSET program) control is transferred to the proper jet-dressing routines of the JETSET LUND program for both systems of quark and di-quark. The program produces the hadronic component of the interaction. When the energy transfer is smaller than the threshold, which for our energy spectrum happens in about 30% of all events, only the kinematics of the final lepton are recorded. The hadrons, unlike the leptons in such cases, do not have high energies in the laboratory system.

The original kinematical routines of the LEPTO program are adjusted to account for nonzero masses of the secondary leptons.

Tau meson decays are handled by the standard routines of JETSET.

D.2 Signal of particles entering the detector through the walls from deep inelastic neutrino interactions in the surrounding rock

Neutrino interactions are generated by the program described in the previous section. The resulting "stable" charged particles are followed until they stop or decay in the matter surrounding the detector, using the GEANT program. Parameters for the tracks entering the detector are written out to a file. A schematic representing this idealized setup of the IMB detector and the surrounding rock is shown in figure 31. The results of these calculations provide a good estimate of the real effects. A more realistic description of experimental conditions is not a technical problem, however

it increases demands on CPU time.

We present here the results of a run based on the neutrino spectrum on the beam axis. Allowing for 5×10^5 interactions in the $5.5 \times 10^5 m^3$ volume of salt surrounding the detector we find 6230 muons entering the detector; 240 are accompanied by pions. In addition, 100 single and 30 multiple pion tracks enter without muons. Including neutral current interactions, which have a cross section of one third of the charged current, we find 260 pion events for 6230 muon events.

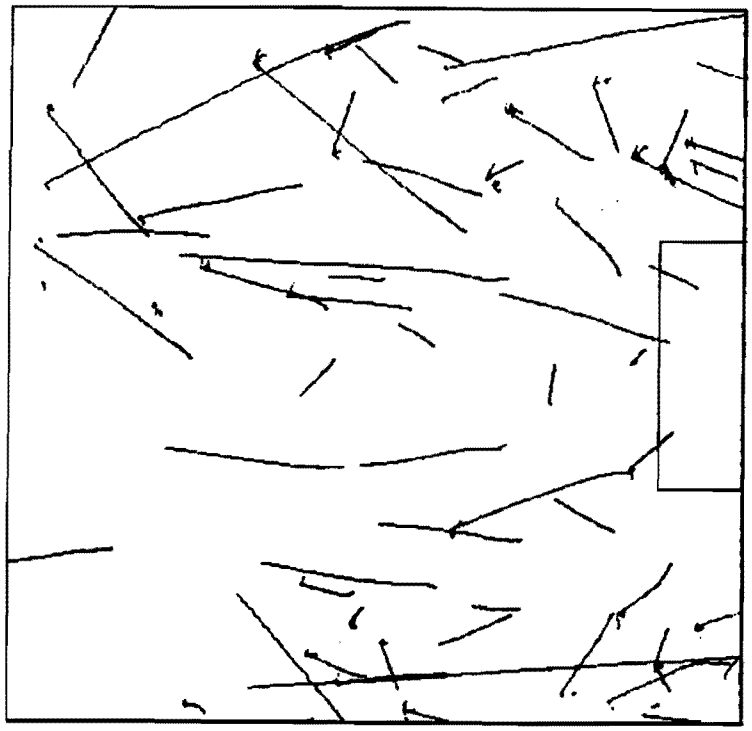

Figure 31: Setup of the IMB detector and the surrounding rock as used by the GEANT program to estimate the number of expected muon tracks entering the detector. Several events generated by the program are also shown.

References

[1] K.S. Hirata et al. *Phys Let B*, 205, 1988.

[2] C. Arpesella. In *Proceedings of the XXIV Int. Conf. on High Energy Physics*, 1988.

[3] W. Gajewski. In *Proceedings of the XXIV Int. Conf. on High Energy Physics*, 1988.

[4] D. Casper et al. Measurment of atmospheric neutrino composition with imb-3 detector. 1990. submitted to Phys. Rev. Lett.

[5] V. Barger and K. Whisnaut. *Phys. Lett. B*, 209, 1988.

[6] J.G. Learned et al. *Phys. Lett. B*, 207, 1988.

[7] G.K. Leontaris and D.V. Nanopoulos. *Phys. Lett. B*, 212, 1988.

[8] A. Ijspeert and P. Sievers. Cern private communication.

[9] R. Bellone et al. *Targets for high intensity beams at CERN.* Technical Report 86/ST/TE/A/113, CERN.

[10] W. Kalbreier et al. *External targets at the SPS.* Technical Report LABII/BT/74-1, 1974.

[11] J.C. Schnuriger and A. Ball. Cern private communication.

[12] Dusseu et al. Technical Report CERN-72-11, CERN.

[13] C. Foos and V. Palladino. Cern-private communication.

[14] C. Foos. Cern-private communication.

[15] H.W. Atherton et al. *Precise Measurements of Particle Production by 400 GeV/c Protons on Beryllium Targets.* Technical Report 80-07, CERN.

[16] A.E. Brenner et al. *Phys Rev D*, 26(7), 1982.

[17] D.S. Barton et al. *Phys Rev D*, 27(1), 1983.